THE ASTROPHYSICAL JOURNAL, 316:1–22, 1987 May 1

PROFILES OF CLUSTERS OF GALAXIES: COSMOLOGICAL SCENARIOS VERSUS OBSERVATIONS

MICHAEL J. WEST, AVISHAI DEKEL,[1] AND AUGUSTUS OEMLER, JR.
Department of Astronomy, Yale University
Received 1986 February 13; accepted 1986 October 22

ABSTRACT

We study rich clusters of galaxies using N-body simulations in comparison with observations. Protoclusters are identified in large-scale simulations which represent a wide range of cosmological scenarios (hierarchical clustering, pancake scenarios, and hybrids, spanning a range of power spectra in flat and open universes), and each cluster is then simulated with high resolution. The density profiles of the simulated clusters (for $\Omega = 1$) are found to be similar, irrespective of the initial conditions. The projected profiles have logarithmic slopes of about -1.8 at the half-mass radius, and they steepen with increasing radius. The velocity dispersion profiles are also similar, and the velocities are quite isotropic. The existence of a universal profile suggests that violent relaxation is efficient at erasing traces of the initial conditions from the cluster profile during the first collapse, while secondary infall does not significantly affect it. Hence, the cluster density profile is not a good indicator of the origin of the large-scale structure in the universe.

Observed luminosity profiles are obtained for a sample of 27 Abell clusters, and a comparison with the theoretical mass density profiles shows good agreement, suggesting that the cluster radial light distribution traces the mass distribution. The theoretical line-of-sight velocity dispersion profiles (for $\Omega = 1$) also agree well with those of five Abell clusters for which reasonably good profiles exist. The profiles of the clusters formed in an open universe are found to be steeper in the inner regions than the observed profiles. Other cluster properties which are most sensitive to cosmology are discussed in subsequent papers.

Subject headings: cosmology — galaxies: clustering — galaxies: formation — numerical methods

I. INTRODUCTION

Different scenarios are possible within the framework of the gravitational instability theory for the formation of structure from small density fluctuations. In the two extremes, the structure either formed by clustering "bottom-up" (Peebles and Dicke 1968) if fluctuations survived on all relevant scales (e.g., isothermal fluctuations, or "cold" dark matter), or by fragmentation "top-down" from supergalactic pancakes (Zel'dovich 1970) if small-scale fluctuations were damped out (e.g., adiabatic fluctuations of baryons, or "hot" dark matter, such as ~ 30 eV neutrinos); hybrid scenarios are also possible (e.g., Dekel 1983, 1984; Dekel and Aarseth 1984). There is an ongoing effort to confront these scenarios with observations, which naturally concentrates on the large-scale objects, such as superclusters and voids, which are still relatively unevolved at present, and hence are expected to reflect directly the cosmological initial conditions. Unfortunately, such studies require many galactic redshifts at faint magnitudes, which makes progress slow and expensive. As an alternative, we study rich clusters of galaxies, for which more data are available. The hope is that some memory of the cosmological initial conditions has survived the cluster collapse and subsequent evolution. This notion is supported by indications that many clusters are dynamically young, based, for example, on their relatively low mean densities and on their tendency for alignment (Bingelli 1982; Dekel, West, and Aarseth 1984; Struble and Peebles 1985).

In the present paper, we focus on the density profiles of clusters, which are obtainable from galaxy number counts, and on velocity dispersion profiles. Based on certain assumptions, the original hope was that the present profiles would be related to the initial conditions (e.g., Doroshkevich 1970; Gunn and Gott 1972; Gott 1975; Gunn 1977; Dekel and Shaham 1980; Dekel 1981; Dekel, Kowitt, and Shaham 1981; Peebles 1982; Hoffman and Shaham 1985) and that this relationship could be obtained semianalytically in the following way.

In the linear regime, if the density perturbation field, filtered on a scale r_s, is a Gaussian process, the typical density profile about a high peak is approximately proportional to the two-point correlation function, in the range of radii $r_s \ll r \ll r_c$, where r_c is a coherence radius that gets larger for higher peaks (Doroshkevich 1970; Dekel 1981; Peebles 1982). For example, if the initial power spectrum is $\langle |\delta_k| \rangle \propto k^n$, the typical profile is $\propto r^{-(3+n)}$. The exact solution (Doroshkevich 1970; Bardeen *et al.* 1986) gives for moderate-amplitude peaks a somewhat steeper profile and smaller r_c. One hopes that at least for the richest protoclusters, there is a range of radii in which such an analysis is valid. (This analysis is useless, however, in pancake scenarios, where clusters form by nonlinear coupling of perturbations on large scales.) Then, assuming spherical symmetry (which might be a poor approximation for moderate peaks though), one can easily calculate the "turnaround profile." The subsequent infall, however, is complicated by "shell" crossing, and the crucial question is whether the final profile is indeed related to the turnaround profile.

In the case of slow, *gradual infall*, Fillmore and Goldreich (1984), extending the rough treatment of Gunn (1977), found self-similar solutions for power-law initial profiles; the power law is roughly preserved if the initial logarithmic slope is steeper than -2 (i.e., $n > -1$), and the final slope is roughly -2 for every initial slope that is less steep ($n \leq -1$). The

[1] Also Racah Institute of Physics, Hebrew University of Jerusalem.

N-body simulations of secondary infall by Dekel, Kowitt, and Shaham (1981) did indeed show that some memory of the initial profiles survives in the final systems, and it was found by Frenk *et al.* (1986) and Quinn, Salmon, and Zurek (1986), using high-resolution N-body simulations of high-density systems dominated by secondary infall ($n \approx -2$), that the final "rotation curve" is quite flat at large radii, corresponding to a $\rho \propto r^{-2}$ density profile in three dimensions, as predicted by the infall similarity solution for $n \leq -1$.

On the other hand, if the collapse is not gradual enough, *violent relaxation* (Lynden-Bell 1967) is expected to erase memory of the initial conditions. It is difficult to derive analytically the profile that arises in a finite system as a result of violent relaxation, but numerical simulations of spheroidal systems (Peebles 1970; White 1976; van Albada 1982; Pryor and Lecar 1983; Farouki, Hoffman, and Salpeter 1983; Villumsen 1984) have shown that if the system is initially cold, clumpy, or aspherical, then it ends up with a certain "universal" profile. Hence, these analytic approximations do not provide a unique prediction for the final density profile.

In this paper, we examine the final density profiles in clusters of galaxies starting with *realistic* initial conditions as they emerge from a wide range of cosmological scenarios. The protoclusters have no spatial symmetries built into them initially, and the final clusters are still dynamically young and of moderate densities, so we cannot tell *a priori* the role of violent relaxation or secondary infall in determining their final profiles. We find that the final density profiles are not very sensitive to the initial conditions, even in clusters that emerge from very different cosmological scenarios. This result indicates that violent relaxation is efficient at erasing any memory of the initial profile and that secondary infall is not important in this case. It also warns us that using the cluster density profile as a cosmological indicator is not very promising.

However, the existence of a universal mass density profile is not entirely discouraging; it raises the interesting question of whether this profile is similar to the observed luminosity profile. In theory, there are several processes that might lead to a radial segregation between the galaxies and the dark matter in clusters. For example, cosmological arguments have recently suggested biased galaxy formation (Davis *et al.* 1985; Kaiser 1984; Bardeen *et al.* 1986; Rees 1985; Silk 1985; Dekel and Silk 1986; Peebles 1986; Dekel 1986*a*; Rees and Dekel 1986), in which bright galaxies do not trace the mass distribution, and the mean mass-to-light ratio is lower in regions of high background density. If this bias occurs inside the protoclusters, one may expect a mass-to-light gradient to be built in from the epoch of galaxy formation, before the clusters collapse. Alternatively, if galaxies are still forming when the clusters collapse, dissipation may cause a further contraction of the galaxies relative to the nondissipative dark matter, and a similar segregation effect would arise. Also, dynamical friction would make the bright galaxies spiral into the cluster centers (Ostriker 1977; Malumuth and Richstone 1984), but this effect is important only in the cluster cores, and perhaps only during the cluster formation, before the galaxies suffer significant tidal stripping (Merritt 1984).

The observational evidence on the relation between the mass profiles and the luminosity profiles is still ambiguous. Kent and Gunn (1981) and Kent and Sargent (1983) have studied the Coma and Perseus clusters by estimating the mass profile from the radial velocities. They claimed that in Coma a constant mass-to-luminosity profile is consistent with an isotropic velocity dispersion, while in Perseus only a nonisotropic velocity model can be consistent with a constant mass-to-luminosity ratio.

We study here the luminosity profiles of 27 Abell clusters and find that they are similar in shape to the theoretical mass profiles obtained in the simulations. The line-of-sight velocity dispersion profiles also agree reasonably well. The velocities in our models are found to be quite isotropic out to at least twice the half-mass radius.

The simulations and the theoretically obtained mass profiles are described in § II, the observed luminosity profiles are presented in § III, and they are compared to each other in § IV. Then a complementary study of the velocities is described in § V. Our conclusions are summarized in § VI. Other cluster properties which are more sensitive to the cosmological initial conditions are discussed in subsequent papers (e.g., West, Dekel, and Oemler 1986*b*; hereafter Paper II; West, Dekel, and Oemler 1986*c*, hereafter Paper III).

II. MODEL MASS DENSITY PROFILES

a) N-Body Simulations

The clusters have been simulated in two steps. First, low-resolution, large-scale cosmological simulations of the different theoretical scenarios have been performed to find the locations of protoclusters and to generate the initial conditions for the second, major step, in which high-resolution simulations of clusters have been performed.

The cosmological simulations have been performed with ~ 4000 equal-mass particles using a comoving N-body code (Aarseth 1984) which integrates directly the Newtonian equations of motion using a softened gravitational potential on small scales. The procedure used here to generate the initial conditions is a generalization of that used by Dekel and Aarseth (1984). The particles were initially distributed uniformly inside a unit sphere, at the points of a cubic grid, so as to initially suppress any undesired small-scale noise. Then the position of each particle (and in the pancake and hybrid simulations, its velocity as well) was perturbed by a superposition of 1000, small-amplitude plane waves, assuming random phases and wave vectors. The wavenumbers were chosen so as to provide a random realization of a given spectrum of fluctuations. This procedure is described in the Appendix. The parameters used in the large-scale simulations are summarized in Table 1. The evolution of each system was followed in the linear regime by the approximation of Zel'dovich (1970), until a stage where the rms density contrast on a scale $\lambda_u = 0.5$ reached ~ 0.25, at which point the cosmological expansion factor, a, was set equal to 1, and the N-body simulation started. The parameters were chosen such that in the pancake simulations, the main pancakes reached singularity at a time stage corresponding to $a \approx 4$. Two random realizations have been performed for each of the following five scenarios: three hierarchical clustering scenarios with power-spectrum indices $n = 0$, -1, -2, a pancake scenario with a truncated spectrum beyond a critical wavenumber, and a hybrid of the two scenarios. For the hybrid scenario, the initial perturbation spectrum was such that the amplitude of the small-scale component was one-half that of the large-scale component at the coherence wavelength. The cold dark matter spectrum of perturbations, near the relevant scales for rich Abell clusters, can be approximated by either the $n = 0$ or the $n = -1$ hierarchical clustering case. All simulations, except model f, assumed

TABLE 1

PARAMETERS OF INITIAL FLUCTUATION SPECTRA[a]

Model	Scenario	n	Adiabatic/ Isothermal	λ_{min}[b]	λ_u[b]	λ_{max}[b]	Ω	a_0[c]
a	Pancake	0	A	0.5	0.5	1	1	5.7
b	Hybrid[d]	0, 0	I, A	0.1, 0.5	0.5	0.5, 1	1	5.7
c	Hierarchical	0	I	0.1	0.5	1	1	11.3
d	Hierarchical	−1	I	0.075	0.5	1	1	11.3
e	Hierarchical	−2	I	0.075	0.5	1	1	11.3
f	Hierarchical	0	I	0.1	0.5	1	0.15	22.6

[a] For details, see Appendix.
[b] Wavelength in units of the radius of the initial sphere of the large-scale simulations.
[c] The expansion factor at which the clusters were studied ($r_0 \approx 0.1$ in the large-scale simulations).
[d] The amplitude jump at λ_u is a factor 2 in $|\delta_k|$.

an Einstein–de Sitter universe ($\Omega = 1$). The simulations of model f assumed $n = 0$ hierarchical clustering in an open universe ($\Omega = 0.15$ at the present epoch) to check for any sensitivity of the results to Ω.

The stages of the simulations that correspond to the present epoch have been determined using the two-point correlation function, $\xi(r)$, in the low nonlinear regime, where $\xi \approx 1$. In the pancake simulations, the slope of the correlation function increases with time and matches the slope of $\gamma = 1.8$ of the observed galaxy correlation function at only a single stage of the evolution, which corresponds to an expansion factor of $a \approx 6$ from the start of the simulation. At the time, the correlation length, where $\xi(r_0) = 1$, is $r_0 \approx 0.1$ in the comoving units used in the simulations ($G = m = 1$, where m is the mass of each particle and the comoving radius of the simulated volume is 1.0). To set the physical scaling, we compare r_0 to the claimed value for galaxies, $r_0 \approx 5\ h^{-1}$ Mpc (Davis and Peebles 1983). With this scaling, the diameter of the simulated system corresponds to $\sim 100\ h^{-1}$ Mpc, and the diameters of pancakes are $\sim 30\ h^{-1}$ Mpc. In the hierarchical clustering simulations, the correlation function grows in a self-similar manner, and hence choosing a particular stage which corresponds to the present epoch is somewhat arbitrary. It was decided to choose the stage in which the comoving correlation length has the same value as in the pancake simulations, $r_0 \approx 0.1$. This occurs at $a \approx 11$ in the simulations done, assuming $\Omega = 1$, and $a \approx 23$ was chosen for the open universe case, at which stage $\Omega \approx 0.15$. As will be demonstrated later, the density profiles obtained from the simulated clusters in the hierarchical scenarios are rather insensitive to the chosen time. Representative projected distributions of particles in the various models, at those stages that correspond to the present epoch, are shown in Figure 1.

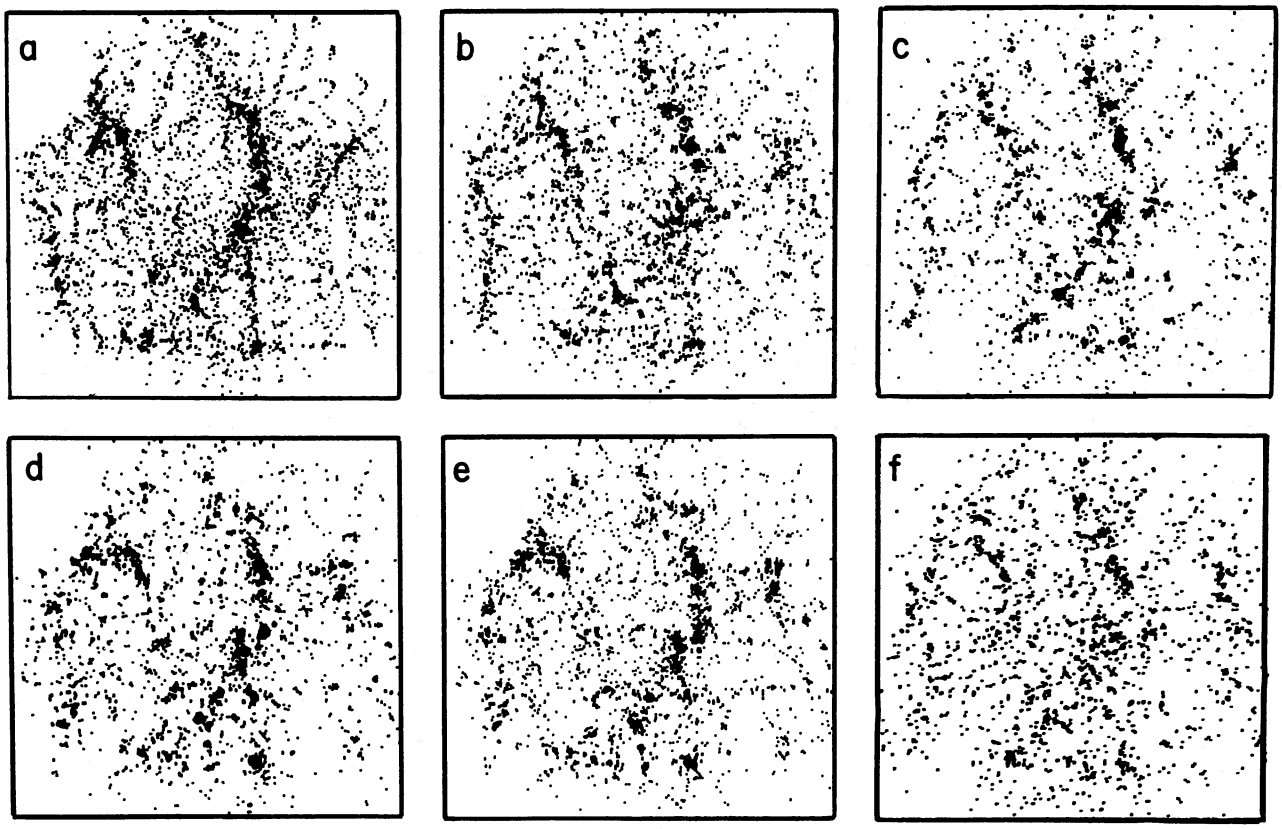

FIG. 1.—Same projection of the different cosmological simulations (see Table 1) at that stage of evolution corresponding to $r_0 \approx 0.1$. Diameter of the spheres corresponds to $\sim 100\ h^{-1}$ Mpc.

Note that the initial fluctuations of the largest wavelength had the same phases in all the scenarios, so similar elongated superclusters are expected to be dominant in all cases. The degree of subclustering reflects the relative importance of small-scale fluctuations in the different scenarios.

The next task is to identify the rich clusters formed in these simulations. Using the above scaling, and given the observed number density of Abell clusters (Bahcall and Soneira 1983), one would expect to find about five Abell clusters of richness class 1, and roughly one of class 2 in each of the simulated volumes. The procedure used here to identify clusters is the simple method of linking near neighbors (Einasto *et al.* 1984; Dekel, West, and Aarseth 1984). For a given value of separation parameter d, all particles closer to one another than this distance are linked together. Particles that are linked to each other, either directly or indirectly, form a cluster. The parameter d is related to the number overdensity, n, at the outer edges of the clusters, via $n = (d/\bar{d})^{-3}$, where $\bar{d}$ is the mean separation between neighbors. The value of d used here to identify the rich clusters in these cosmological simulations corresponds to an overdensity of ~ 35 at the edges of the clusters. A further requirement, viz. that each cluster thus identified contain a certain minimum number of particles, has been imposed to focus as much as possible on those clusters which should be representative of Abell clusters of richness class 1 or greater. Clusters identified using this procedure are found to contain typically 30–50 particles, each corresponding to mass $\sim 2.7 \times 10^{13}\ M_{\odot}$. However, because the aim here is to study the detailed structure of these clusters, such few particles of such large mass cannot provide sufficient resolution on small scales.

It is for this reason that the second, high-resolution step has been taken to create the final cluster models used in the later analysis. Having identified the locations where rich clusters form for a given set of initial perturbations in the different cosmological simulations, new simulations have been performed using these same initial perturbations, but now modeling smaller volumes centered on the locations of each of the five richest clusters found in each of the large-scale simulations. In this way the resolution can be greatly increased, since by concentrating on the relatively small volume around each cluster, the mass of each individual particle in the new simulations can be much smaller, and more of the particles in the simulated volume eventually ended up in the cluster itself rather than in other surrounding structures. Simulations with ~ 1000 particles have been run for each cluster using a noncomoving version of the Aarseth code. The initial radius of these individual cluster simulations corresponds to 45% of the initial radius of the large-scale cosmological simulations, $r_c = 0.45$ in the comoving units of the simulations. This volume size was chosen since it is sufficiently small to achieve the desired high resolution, yet sufficiently large that it still includes the effects of the surrounding structure. As a check, several preliminary simulations were run with larger volumes, and it was found that no significant differences resulted in the structure of the clusters (see § II*d*). Assuming a mean luminosity density in the universe of $2.3 \times 10^8\ h\ L_{\odot}\ \mathrm{Mpc}^{-3}$ (Kirshner *et al.* 1984), each particle in these simulations should represent roughly an L^* galaxy ($L^* \approx 10^{10}\ L_{\odot}\ h^{-2}$) at those stages of the simulations corresponding to the present epoch, where $r_0 \approx 0.1$. Figure 2 shows projections of several typical clusters formed in the different scenarios. To illustrate the effects of the different initial perturbation spectra, we show in each column a cluster which formed in a similar location in the different large-scale simulations. Thus the apparent differences in the visual appearance of this cluster formed in the pancake, hybrid, and ($n = 0$) hierarchical clustering scenarios reflect the differences in the small-scale component of the initial perturbation spectrum, while the differences seen in the $n = -1$ and $n = -2$ hierarchical clustering simulations demonstrate the effects of having more power on large scales.

b) Obtaining the Density Profiles

Three orthogonal, two-dimensional projected views of each of the 10 simulated clusters per cosmological scenario have been used. A cubic volume with origin at the center of the simulated spherical volume has been cut to ensure equal depth along the line of sight. The cluster center in each case is taken as the location of the density maximum of the projected particle distribution within this cube, as determined from an iterative count procedure in square grid cells. In all cases the cluster center determined by this procedure agrees well with that determined from visual inspection of the particle distribution.[2] Visual inspection has also been used to identify any clusters for which there is another very nearby cluster or group which might confuse the analysis. In such cases, all particles within the small region around the undesired cluster have been removed from the field of view. This procedure was used in order to resemble as much as possible the procedure used by observers to obtain the observed profiles. It was required only infrequently. A mean mass density of background matter has been determined for each simulation by simply dividing the total number of particles contained within the cubic volume by the projected area. This procedure may slightly overestimate the true background level; however, it is a simple way of approximating the procedure used by observers to determine the local background density (see § IV). The density profiles for each projected view of each cluster have then been determined by computing the total surface mass density contained within a set of concentric circular rings, and subtracting the appropriate background contribution. The width of the rings has been slowly varied in a systematic way, so as to try to keep the number of particles in each ring approximately constant, ~ 20 particles per ring. This has been done by spacing the ring boundaries uniformly in ln (r). The profiles have been computed out to the radius at which the mass density within the ring, after subtracting the background contribution, first falls to zero. The total cluster mass is then taken as the sum of the masses of all the particles contained within this radius. To compare with the observations, we use the unit M^* which is defined to be the total mass associated with an L^* galaxy. The surface density profiles, $S(r)$, have been computed in two ways: (*a*) in physical units, with the density in $M^*\ (h^{-1}\ \mathrm{Mpc})^{-2}$, and radius in h^{-1} Mpc, and (*b*) in dimensionless units, with the masses and radii normalized in terms of the total projected cluster masses and the projected half-mass radii, so as to facilitate a more direct comparison between the shapes of the profiles for different clusters.

[2] Beers and Tonry (1986) have recently claimed that the density profile obtained for clusters, especially the existence of a core, is quite sensitive to the choice of cluster center. Be that as it may, the procedure which we have adopted here is similar to that used for the observed clusters, which is important since a direct comparison between the theoretical and observational data is desired. Since the same procedure is used in all cases, any differences between the profiles of clusters formed in the different cosmological scenarios can be regarded as real.

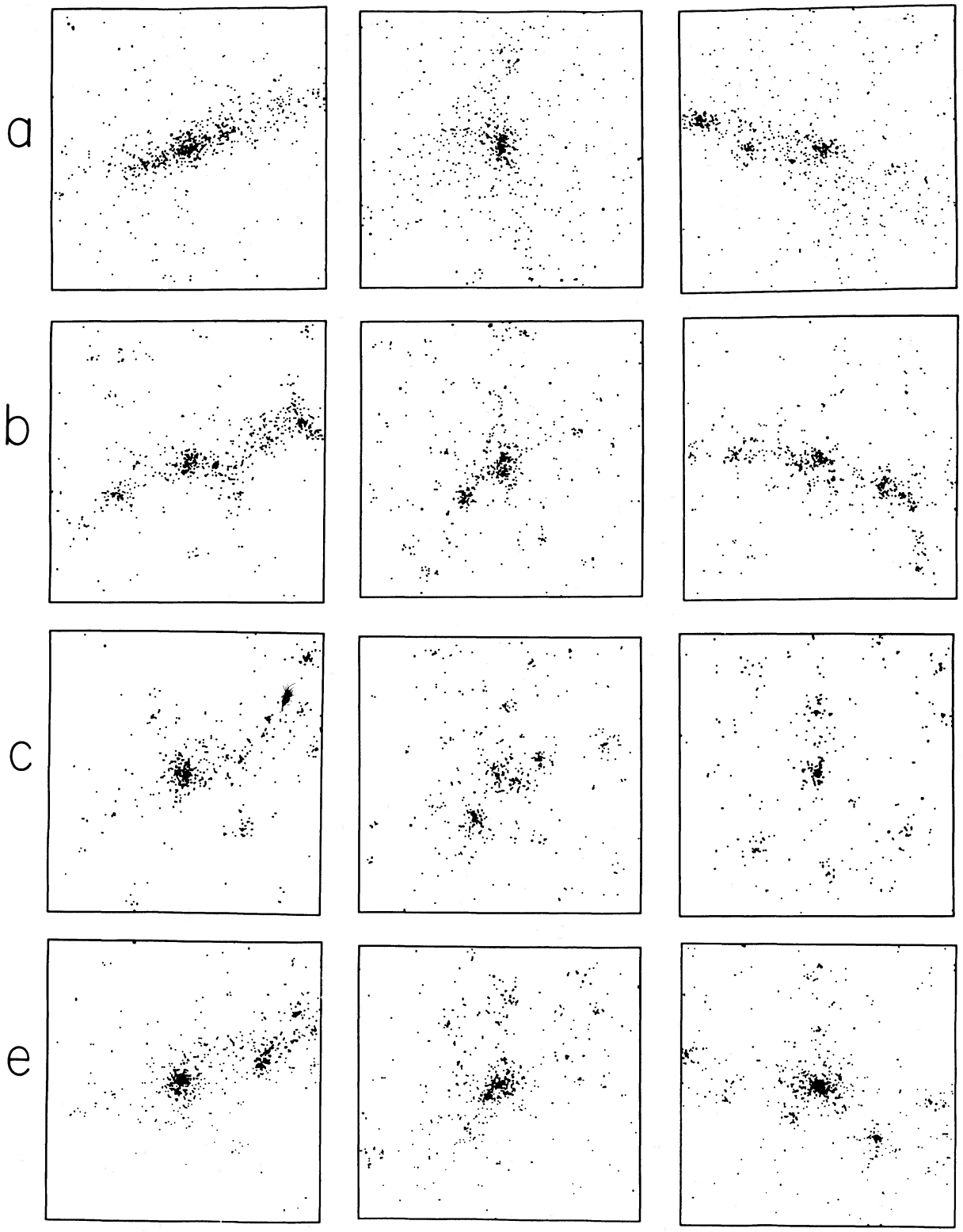

FIG. 2.—Projected views of representative clusters formed in the different cosmological scenarios (see Table 1). Clusters along each vertical column have formed in a similar position in space. Length of each box corresponds to 20 h^{-1} Mpc (which is less than one-half the diameter of the simulated sphere around each cluster.

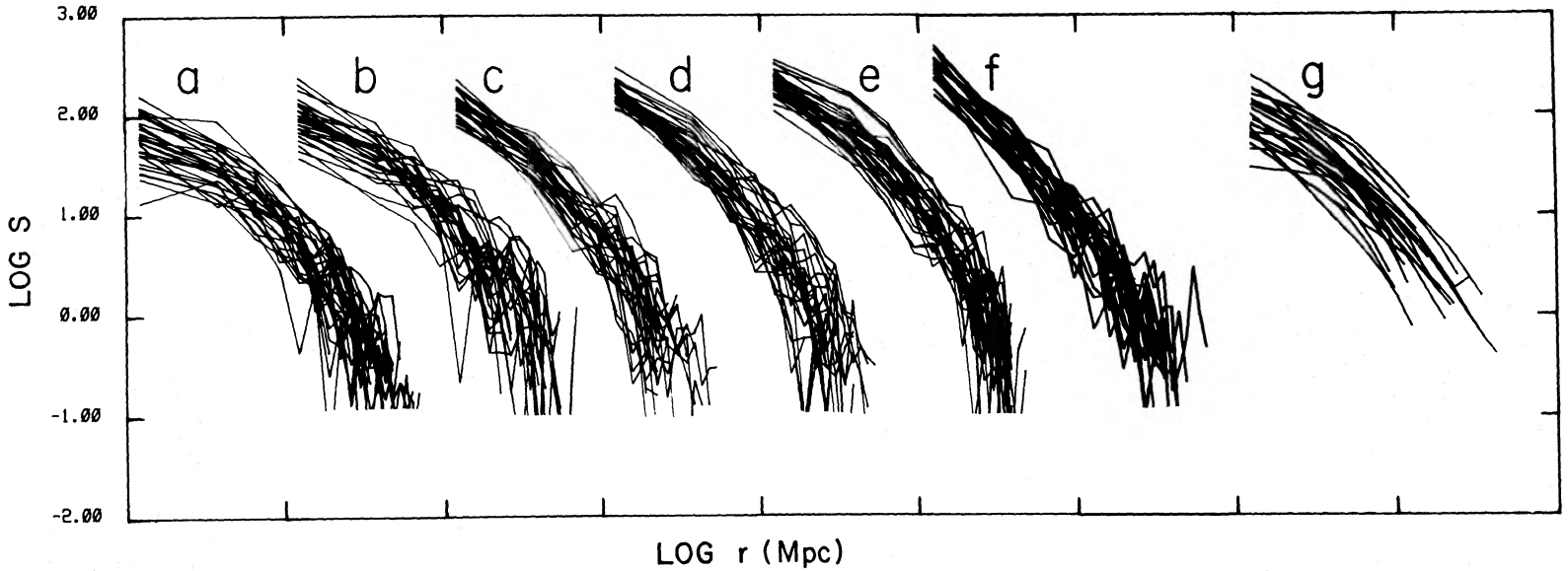

FIG. 3.—Cluster density profiles in physical units; density in M^* $(h^{-1}$ Mpc$)^{-2}$, and radius in h^{-1} Mpc. (*a*)–(*f*) Mass density profiles in the simulated clusters of the different scenarios (Table 1). (*g*) Surface brightness profiles of the sample 27 Abell clusters. Lines shown in (*g*) are the smooth curves drawn through the observational data points for each cluster in Fig. 12. Tick marks are spaced at intervals of 1 in log $(r/1\ h^{-1}$ Mpc). The profiles of the different scenarios are shifted by 1 in log *r* relative to each other.

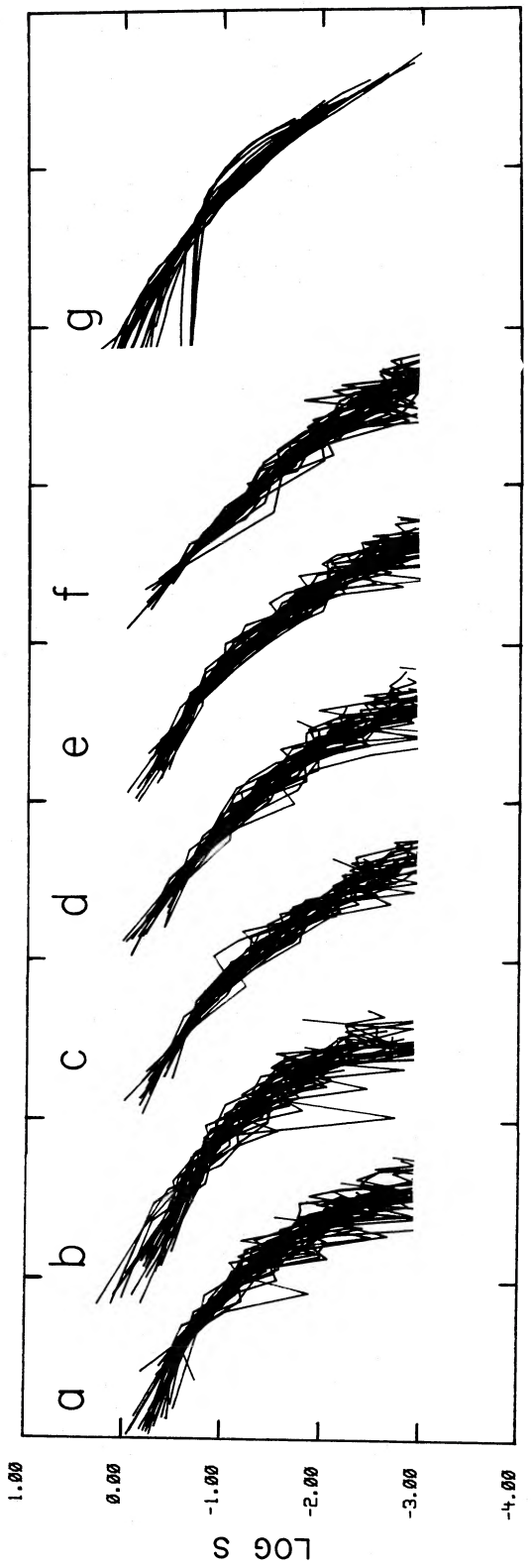

FIG. 4.—Normalized density profiles, as described in the text. Curve labels are the same as in Fig. 3. Tick marks are spaced at intervals of 1 in $\log (r/R_{50})$. Profiles of the different scenarios are shifted by 1 in $\log r$ relative to each other.

Finally, we calculate several simple quantities to help characterize the shapes of the density profiles. Local logarithmic slopes are defined by

$$\alpha_i = \left[\frac{d(\log S)}{d(\log r)}\right]_{R_i}, \quad (1)$$

where R_i is the projected radius that encompasses i% of the total mass. We measure α_{25}, α_{50}, and α_{75}. In addition, a measure of the degree of central concentration is the concentration index C (Butcher and Oemler 1978) which is defined by

$$C = \log (R_{60}/R_{20}) . \quad (2)$$

This quantity should be sensitive to any core structure in the profiles.

c) Results

In Figure 3, the density profiles computed in physical units are shown for each of the simulated clusters at the stage of evolution corresponding to the present epoch. Similarly, in Figure 4, the normalized profiles are presented. It is evident from these figures that the shapes of the profiles are quite similar. This can be seen even more clearly in Figure 5, where best-fit curves to the data are compared for the normalized profiles. These curves are a fourth-order power series whose coefficients were determined by minimizing χ^2. In Table 2, the slopes α_{25}, α_{50}, and α_{75} of these profiles are presented for comparison. Similarly, in Figure 6 we show the distribution of the concentration index C for the different clusters. It is interesting to note that in addition to agreeing in shape, the scaling of these profiles is not drastically different, the typical half-mass radius of these clusters ranges roughly from ~ 0.5 to $1\ h^{-1}$ Mpc, depending on the cosmological scenario (Paper II).

The temporal evolution of the density profiles can be examined in Figure 7, where the best fits to the profiles at three different times are presented for two representative cases; the pancake simulation and the $n = 0$, $\Omega = 1$ hierarchical clustering simulation. In the pancake scenario, the profiles steepen in time, as the steepening of the correlation function (see Dekel and Aarseth 1984) would indicate; recall that the present time is uniquely determined by fitting the slope of the correlation function to the observed slope. In the hierarchical scenario, the profile shapes remain self-similar, ensuring us that our choice of the present time in this case has no effect on our conclusions.

TABLE 2

MEAN SLOPES FOR PROJECTED DENSITY PROFILES

Model	Scenario	α_{25}	α_{50}	α_{75}
a.....	Pancake	−1.0	−1.8	−2.3
b.....	Hybrid	−0.9	−1.7	−2.4
c.....	Hierarchical ($n = 0$)	−1.1	−1.8	−2.3
d.....	($n = -1$)	−1.1	−1.8	−2.3
e.....	($n = -2$)	−1.0	−1.9	−2.4
f.....	($n = 0$, $\Omega = 0.15$)	−1.4	−1.8	−2.1
g.....	Abell clusters	−1.1	−1.7	−2.2

d) Interpretation

The fact that a wide range of initial conditions results in the same universal profile suggests that violent relaxation is responsible for erasing traces of the initial conditions from the final radial mass distribution in clusters. Using N-body simulations of the dissipationless collapse of galaxies, van Albada (1982) and May and van Albada (1984) showed that for spherical systems, violent relaxation is able to produce a universal mass density profile, provided that the systems are initially clumpy. This should be the case for those of our clusters formed via the hierarchical clustering of smaller clumps. Similarly, Villumsen (1984) showed that initially smooth systems can also undergo significant violent relaxation, provided that these systems are aspherical in shape. This should be relevant

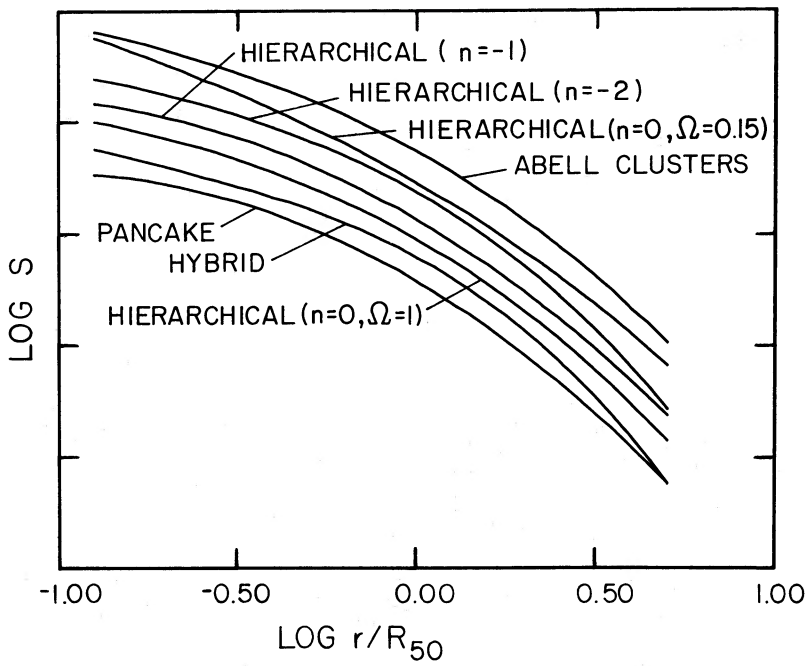

FIG. 5.—Comparison of best-fit curves for the profiles shown in Fig. 4. Fitting function was a fourth-order power-series with coefficients determined by minimizing χ^2. Curves have been shifted relative to each other by 0.2 in log S.

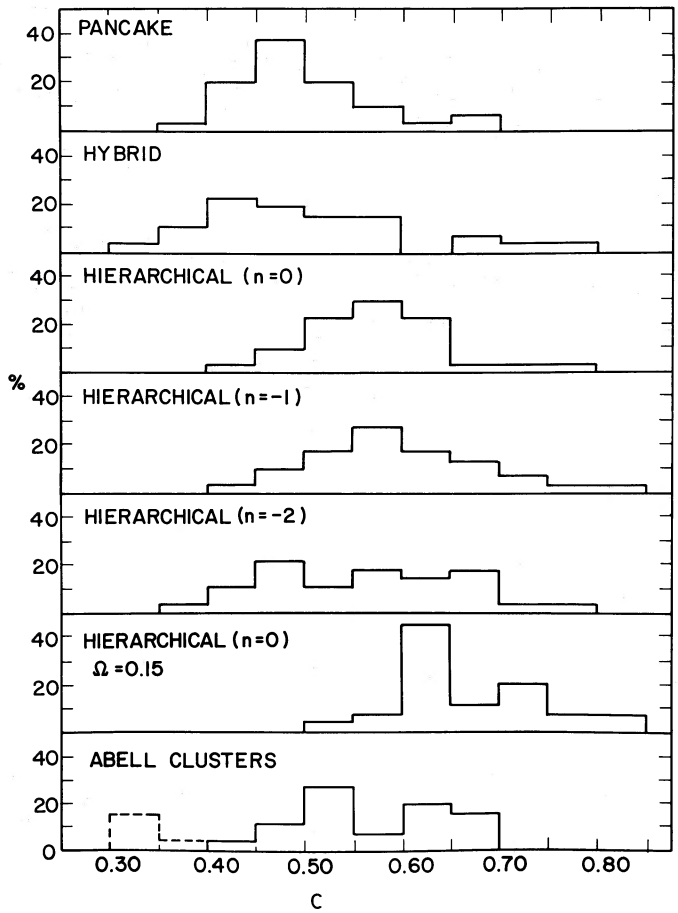

FIG. 6.—Distribution of the concentration index C for the clusters

for those clusters formed in the pancake scenarios. Thus, although the clusters in the different scenarios have formed with varying degrees of initial asphericity and clumpiness, it seems that the process of violent relaxation plays an important role in all cases, leading to a universal profile.

Secondary infall, which may preserve the initial conditions, seems to be unimportant here. To ensure that secondary infall has not been suppressed by having simulated too small a volume, we have rerun three of the clusters of the $n = -2$ hierarchical clustering scenario, this time simulating a larger region, of radius $r_c = 0.7$, hence allowing for more extended regions around the cluster to participate in any infall. In Figure 8, the resultant mean profile for these clusters is compared with the mean profile originally obtained using a sphere of radius $r_c = 0.45$. The profiles are quite similar, indicating that our original simulations do not miss significant secondary infalling mass, even in the $n = -2$ case, where the perturbation power on large scales is greatest.

Other simulations of hierarchical clustering scenarios (Frenk *et al.* 1986; Quinn, Salmon, and Zurek 1986), aimed at reproducing the "rotation curves" of spiral galaxies via the three-dimensional mass/radius profile of their dark halos, $[M(r)/r]^{1/2}$, do indicate some sensitivity of the final profiles to the initial power spectrum (although not as strong as predicted by the infall self-similarity solutions). In particular, they obtain flat "rotation curves" for $n = -2$. In Figure 9, we show for comparison the three-dimensional $[M(r)/r]^{1/2}$ profiles for 10 arbitrary clusters or our $n = 0$ and $n = -2$ simulations. The average profiles of these clusters for each case are shown in Figure 10. They are obtained after scaling the mass of each cluster to units of its total mass (defined at the radius where the mean angle-averaged density equals the mean density of the background) and the radius to units of its half-mass radius. It is evident that the "rotation curves" in our $n = -2$ clusters

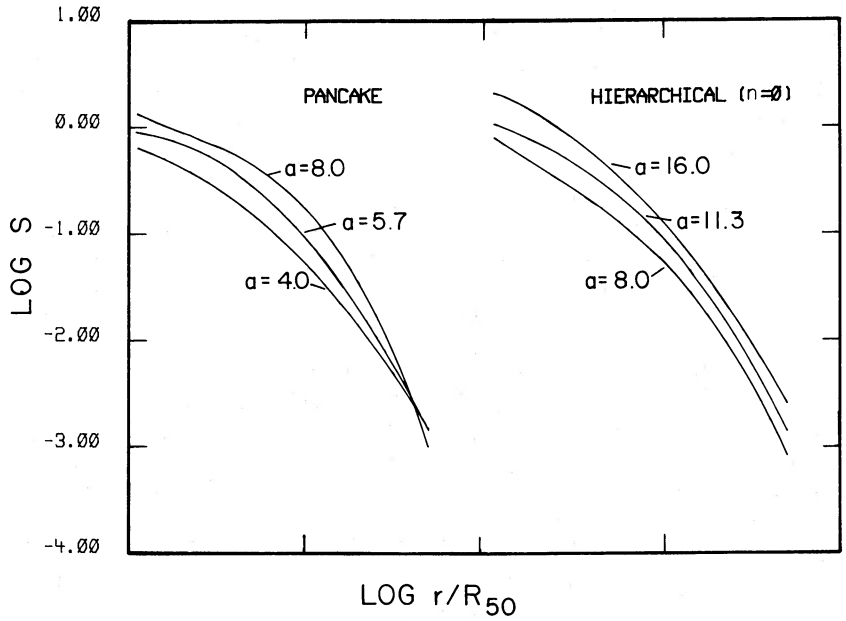

FIG. 7.—Temporal evolution of the density profiles for two representative cases: (*a*) pancake scenario, and (*b*) $n = 0$ hierarchical clustering scenario. These curves are best fits to the profiles. Each profile is labeled by the expansion factor at which it was determined. Curves have been shifted by 0.2 in log S.

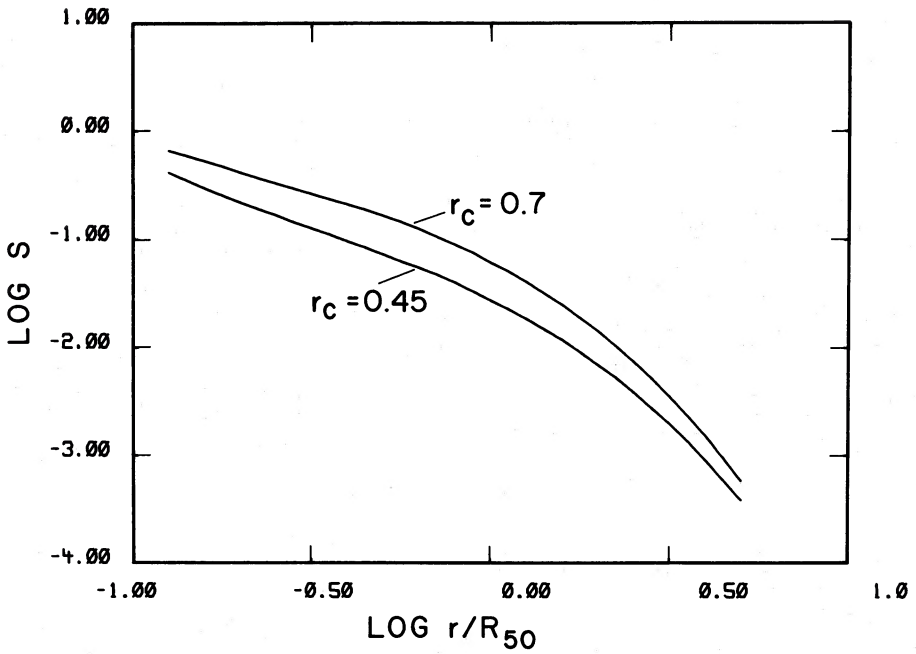

FIG. 8.—Effect of changing the size of the simulated volume. Curves are best fits to the density profiles for three clusters simulated in the $n = -2$ hierarchical clustering scenario using $r_c = 0.45$ and $r_c = 0.7$. Top curve has been shifted upward by 0.2 in log S.

decrease much as the $n = 0$ ones out to several half-mass radii. Hence, the similarity seen before between the two-dimensional profiles of the clusters within the inner few megaparsecs reflects a similarity in three dimensions.

A plausible interpretation is that our clusters relax more violently and suffer less secondary infall than the galactic halos in the other simulations. This may be due to a basic difference between galaxies and clusters. The galaxies, being of higher densities have collapsed well before the present epoch and have subsequently accreted a significant portion of their mass via secondary infall, while the clusters, being of relatively low densities, have collapsed only recently, and thus significant secondary infall has not yet occurred. Other possible explanations for the difference might be, for example, differences in the ways we set the initial conditions or the number of particles simulated per cluster. A detailed comparison between the processes of violent relaxation and secondary infall will be the subject of another paper.

The final profiles do show some slight dependence on Ω. The clusters formed in the case of an open universe are somewhat more centrally concentrated, as can be seen in the inner regions of the profiles shown in Figures 3*f* and 4*f*, and is reflected in the values of the concentration index C and α_{25}. In an open universe, clusters will have stopped growing when the universe entered the free expansion phase; they are therefore smaller in size relative to the comoving volume, and have density profiles which are more steeply decreasing. The clusters formed in an open universe will have had a longer time to evolve until the point where the large-scale distribution of matter matches the observed correlation function, so their cores are at a more dynamically evolved state than their counterparts in an Einstein-de Sitter universe. However, it is important to bear in mind that the simulations used here have not attempted to incorporate more detailed physical processes, such as dynamical friction, mergers, and mass segregation, which may affect these profiles in the innermost regions.

Thus, these results seem to indicate that once clusters of galaxies collapse, their radial mass distribution becomes essentially independent of the surrounding cosmological initial conditions from whence they arose. Indeed, the profiles obtained here are not very different from those found by Peebles (1970) and White (1976) in their simulations of spherical, isolated clusters, which did not include the treatment of any surrounding cosmology.

III. OBSERVED LUMINOSITY PROFILES

To compare with the model clusters, we have assembled data about the structure of real clusters of galaxies. Since most of the data are in that form, we shall confine ourselves to observations of the radial distribution of cluster galaxies in two dimensions. A survey of the literature gives the impression that the radial profiles of clusters are poorly known. It is possible to find very large differences between the profiles of one cluster as determined by two or more workers. Dressler (1978) has found a factor of 2 discrepancy between the core sizes of clusters determined by himself and by Bahcall (1975). Assertions about the general form of the surface density distributions vary widely. Oemler (1974) claimed that his cluster profiles were consistent with the results of N-body collapse models, whose surface densities vary as r^{-3} in their outer parts. At other extremes, Yahil (1974) found an r^{-1} dependence, with (possibly) an isothermal core at small radii.

The most important reason for these disagreements is the necessity to correct for background and foreground galaxies. Although unimportant in the cluster cores, background galaxies dominate the galaxy counts at large radii. Because clusters fade slowly into the background, clusters (at least nearby) subtend a large angular scale, and the clumpy distribution of background galaxies, it is very difficult to estimate the background accurately. Particularly when the galaxy distributions are determined by eye counts, as were most of those in the literature, there is a strong temptation to stop counting at too

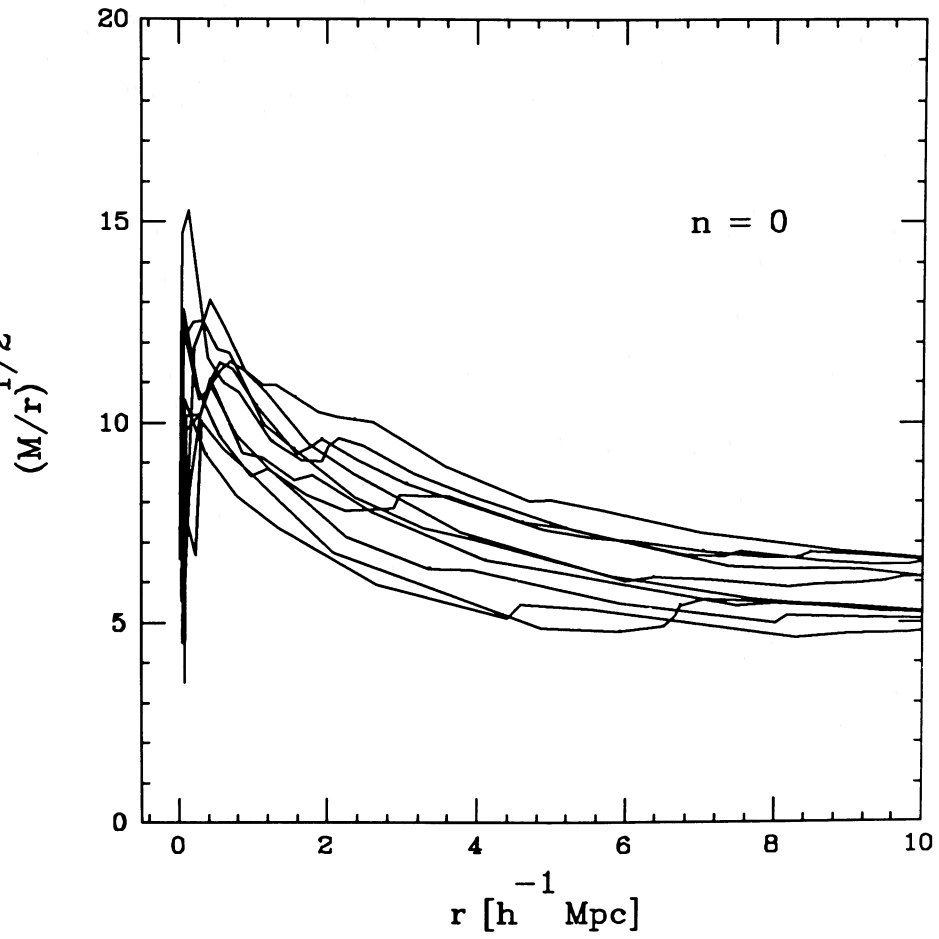

FIG. 9a

FIG. 9.—Three-dimensional mass profiles ("rotation curves") in physical units for 10 arbitrary clusters in each of the hierarchical simulations. (*a*) $n = 0$; (*b*) $n = -2$.

small a distance from the cluster center. This results in an overestimate of the background and an abnormal truncation of the cluster profile.

That the situation is not hopeless, however, can be seen from Figure 11*a*, which presents four determinations of the profile of the Coma Cluster, one of the best studied clusters. The solid line is the radial distribution of galaxies with measured velocities near that of Coma, as determined by Kent and Gunn (1982). This velocity discrimination eliminates almost all foreground and background contamination, and no correction for contamination has been applied to this profile. However, because the cluster is superposed on a finite mean cosmic density of galaxies, this profile represents an upper limit to the true cluster distribution. The dashed and dotted lines represent the profiles determined by traditional eye galaxy counts, performed by Omer, Page, and Wilson (1965) and Zwicky (1937). Background corrections have been applied to both; because the former counts go much deeper, the corrections to these are much larger than to Zwicky's counts. Finally, the points with error bars represent the cluster surface brightness distribution (or equivalently, the luminosity-weighted galaxy distribution) measured by Oemler (1974). The galaxy distribution was determined by an automatic search program; the background correction was made using a mean relation of field galaxy density versus magnitude determined from many regions.

The four profiles agree very nicely. There is a slight tendency for the Kent and Gunn profile to be more extended than the others, but the effect is small, confined to the outermost points, and consistent with this profile being an upper limit to the true distribution. The general form of the profile is compared to various proposed profile shapes in Figure 11*b*. A mean of the four determinations of the profile is represented by open circles. The solid line represents the average profile from the simulated clusters. The dashed line is an $r^{1/4}$ law fit of the type favored by Dressler (1978), and the dotted line represents Yahil's proposed distribution. The last is obviously a poor representation of the data. The former fits reasonably well over the observed range in radii (the $r^{1/4}$ law fits may clusters more poorly). We conclude from this comparison that clusters of galaxies are finite and bounded (as would not be the case if surface density varied as r^{-1}) and that it is possible, with careful work, to accurately determine their profiles.

We have examined the entire body of data in the literature on cluster profiles. Unfortunately, few clusters have been studied as carefully as has Coma. We have concluded that, with few exceptions, no cluster profile could be trusted if it were based on only one determination. From the extant data, we have found 27 clusters in whose profiles we have some confidence. These are listed in Table 3 and the individual profiles are shown in Figure 12. For each cluster we list the sources

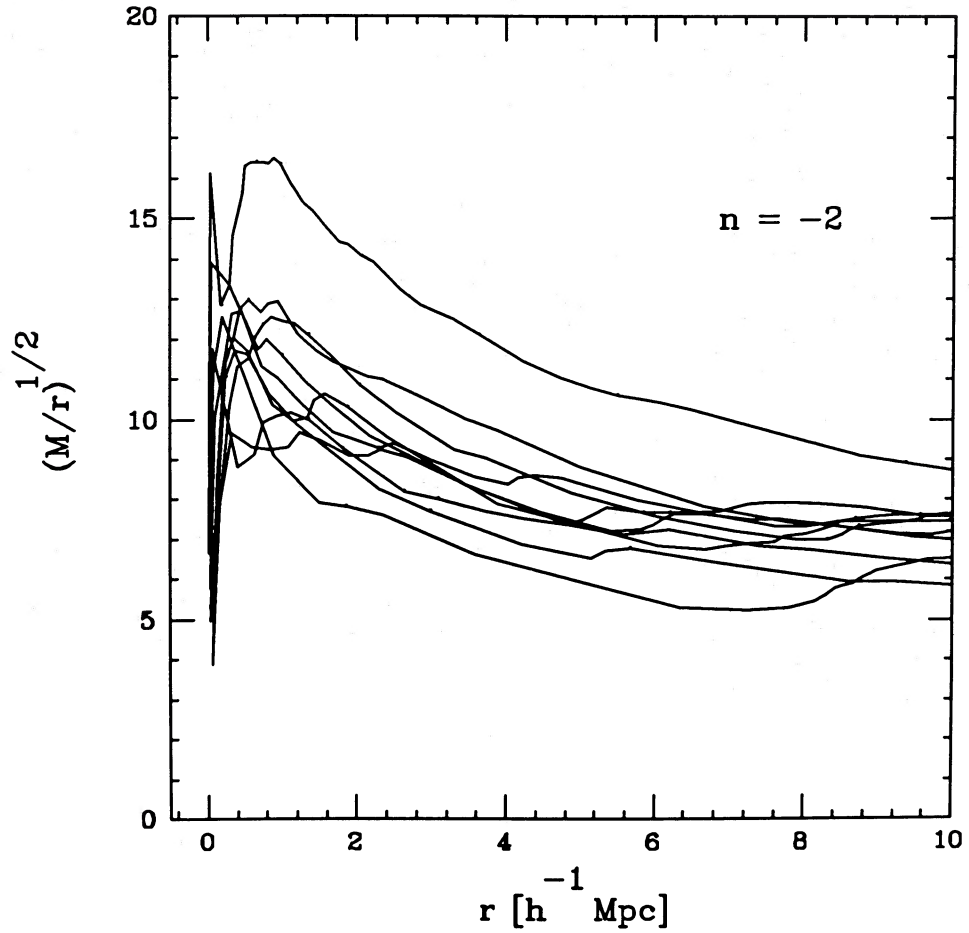

FIG. 9*b*

TABLE 3

CLUSTERS OF GALAXIES WITH RELIABLE PROFILES

Cluster	C	R'_{50}	References
Coma	0.53	51.	1, 2, 3, 4
Corona Borealis	0.64	14.	5
Fornax	0.64	75.	6
Hercules	0.33	21.	2, 7, 8
Hydra	0.61	75.	9, 10, 11
Perseus	0.68	59.	4, 12, 13
Virgo	0.30	229.	14
Abell 154	0.65	31.	8, 9, 15
Abell 168	0.67	42.	8, 15
Abell 194	0.47	28.	2, 7, 16
Abell 400	0.48	29.	2, 9, 15
Abell 401	0.60	21.	8, 9, 16
Abell 539	0.54	14.	2, 15, 17
Abell 665	0.47	7.5	2, 8
Abell 1228	0.33	18.	1, 7, 17
Abell 1314	0.43	15.	2, 7
Abell 1367	0.33	23.	2, 9, 13
Abell 1413	0.62	7.1	2, 8, 18
Abell 1795	0.67	22.	9, 16
Abell 1904	0.53	18.	2, 9, 16
Abell 2029	0.63	25.	8, 9, 16
Abell 2197	0.32	28.	2, 7, 9
Abell 2199	0.53	32.	2, 9, 19
Abell 2218	0.59	11.5	8, 20
Abell 2255	0.57	19.	9, 17
Abell 2256	0.51	19.	8, 9, 15
Abell 2670	0.50	8.4	2, 8

of the profile and several parameters: R_{50} and the concentration index C of the galalaxy distribution. Values of C range from $\sim$0.30 for uniform density clusters to $\sim$0.65 for the most centrally concentrated clusters. We have redetermined the profiles of four clusters for this paper. Automated machine counts of galaxies in A2255 and eye counts of galaxies in the other clusters were made using 10″ × 10″ 098 plates obtained on the Palomar 1.2 m Schmidt telescope. Rough values of the total luminosity have been determined for most of these clusters, for use in computing their density profiles in physical units. More precise values of the total luminosities will be published in Paper III.

The combined profiles of all 27 clusters are shown in Figures 3 and 4. It is apparent that there is a fairly small, but distinct, subset of clusters which have markedly different profiles from the others, these clusters appearing to be of rather uniform density over a large range of radii. Their galaxy populations are also unusual, being much richer in spiral galaxies than

NOTES TO TABLE 3

REFERENCES: (1) Kent and Gunn 1982. (2) Oemler 1974. (3) Omer, Page, and Wilson 1956. (4) Zwicky 1957. (5) Zwicky 1956. (6) Duus 1977. (7) Butcher and Oemler 1978. (8) Dressler 1978. (9) Baier and collaborators. See Baier 1978. (10) Kwast 1966. (11) Zwicky 1937. (12) Bahcall 1974. (13) Kent and Sargent 1983. (14) de Vaucouleurs, de Vaucouleurs, and Corwin 1976. (15) Dressler 1980. (16) Bahcall 1975. (17) Remeasurement for this paper. (18) Noonan 1972. (19) Bahcall 1973. (20) Butcher and Oemler 1984.

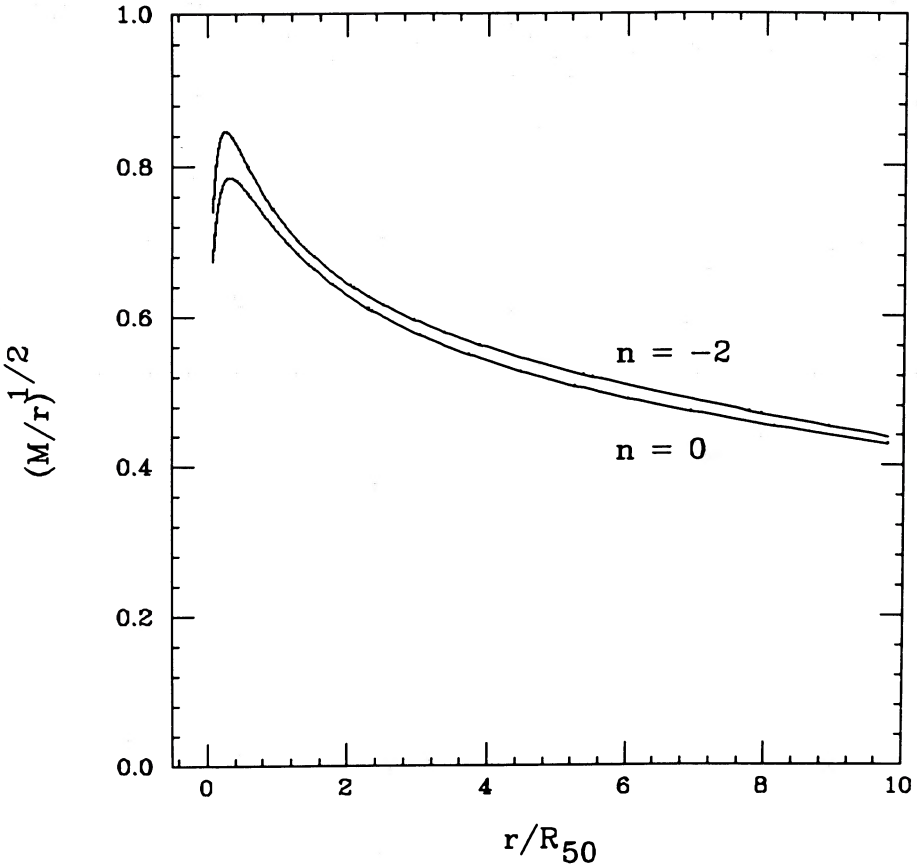

FIG. 10.—Average three-dimensional mass profiles ("rotation curves") based on 10 clusters in each of the hierarchical simulations. The mass is in units of the half-mass of each cluster, and the radius is in units of the half-mass radius of each cluster.

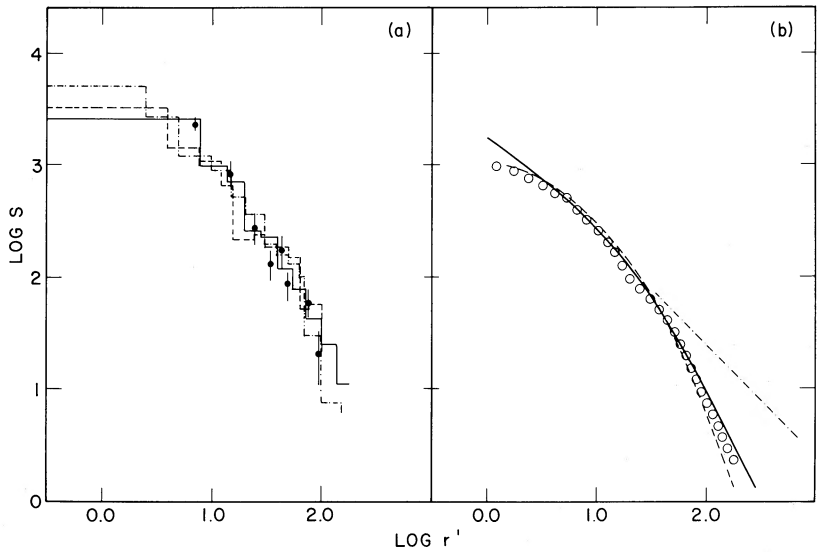

FIG. 11.—(*a*) Four independent determinations of the mean profile of the Coma cluster. (*b*) Comparison of the mean profile from (*a*) with various proposed profile shapes. Circles represent the mean profile; solid line represents the average profile from the simulated clusters; dashed line is an $r^{1/4}$ law fit; dotted-dashed line represents Yahil's proposed distribution.

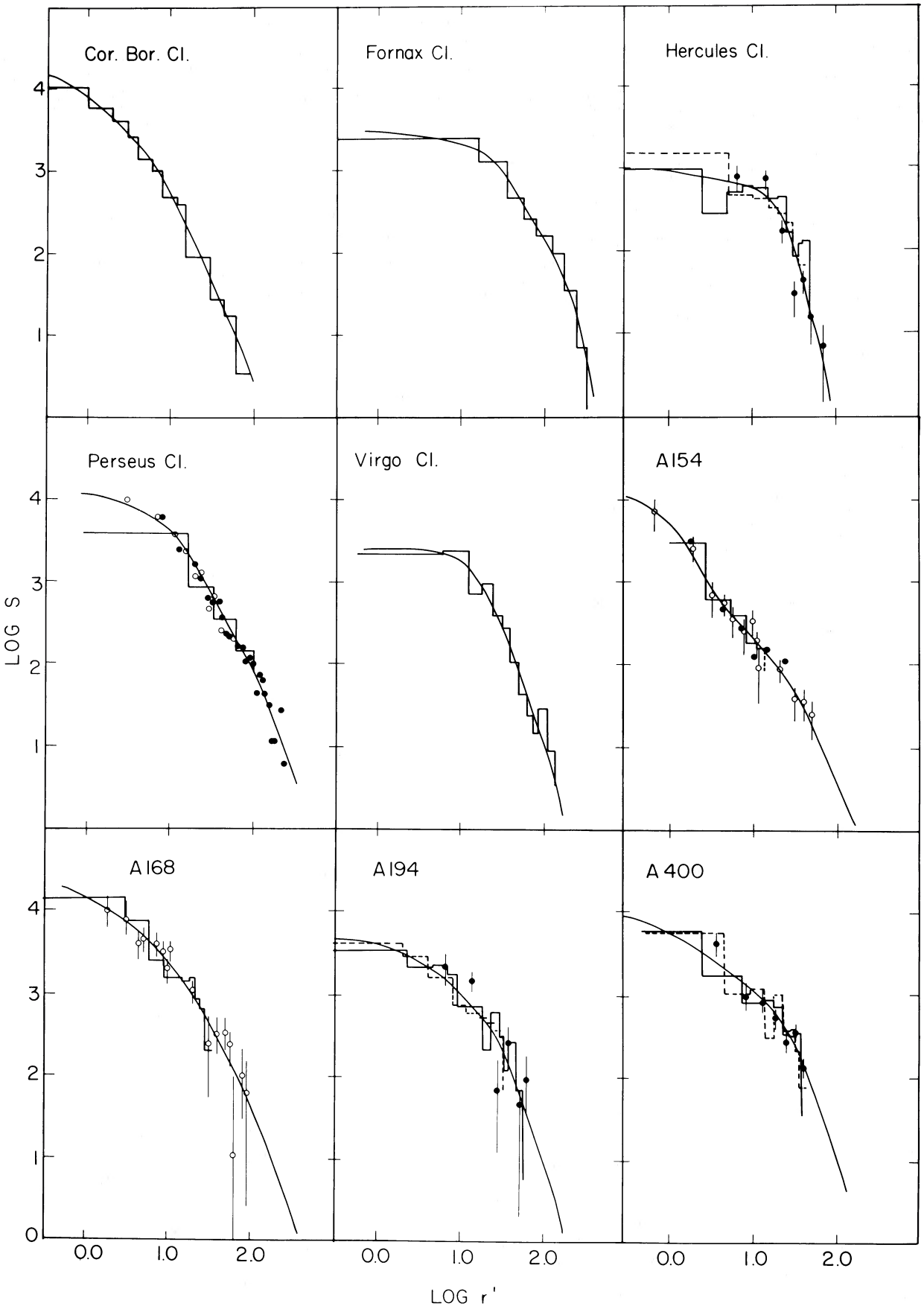

FIG. 12.—Galaxy surface density profiles of the observed clusters. Vertical scaling is arbitrary. Symbols used for the individual profiles correspond to the order of references in Table 3 as follows: first reference, filled circles; subsequent references (in order), open circles, solid line, dashed line.

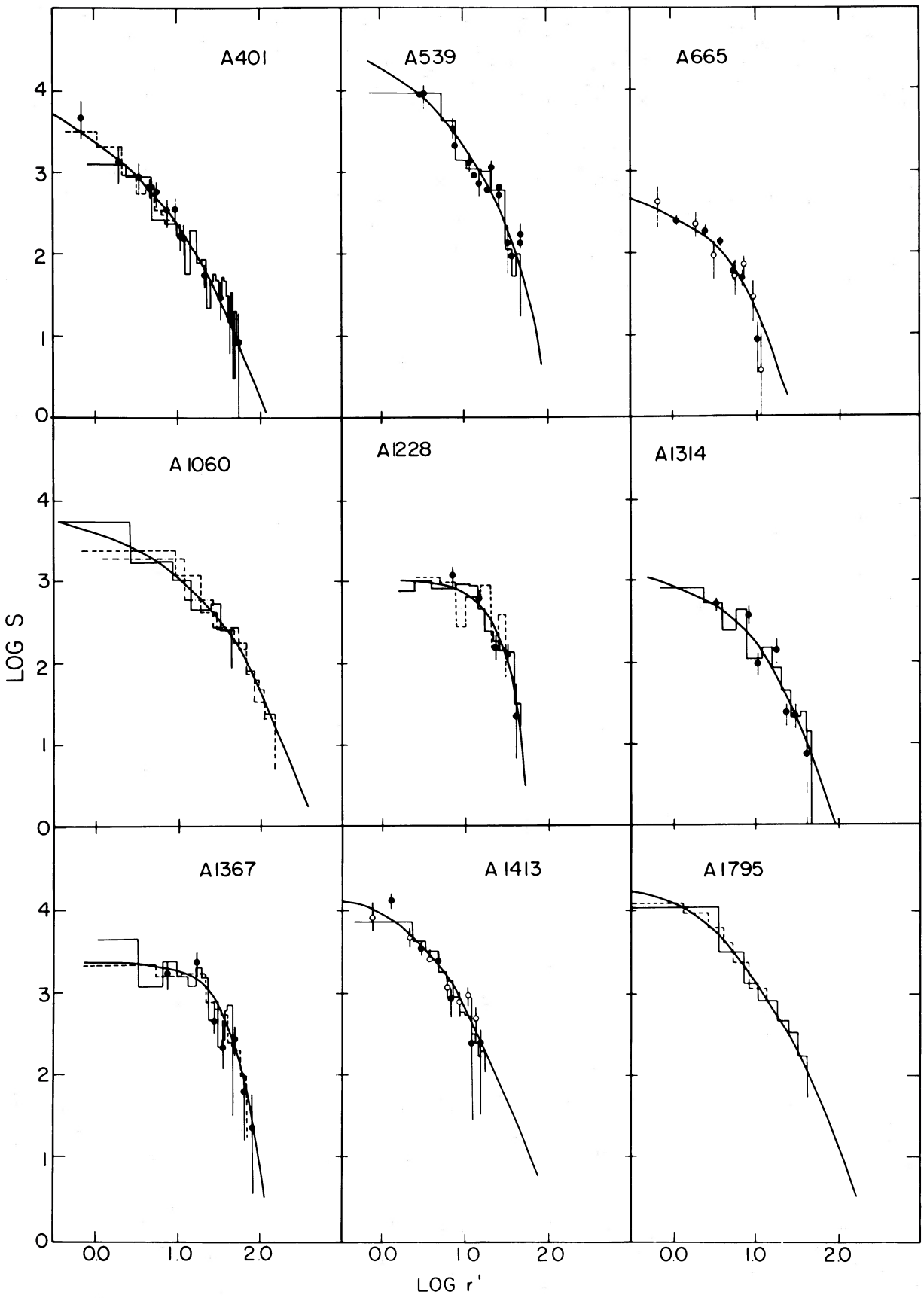

FIG. 12.—*Continued*

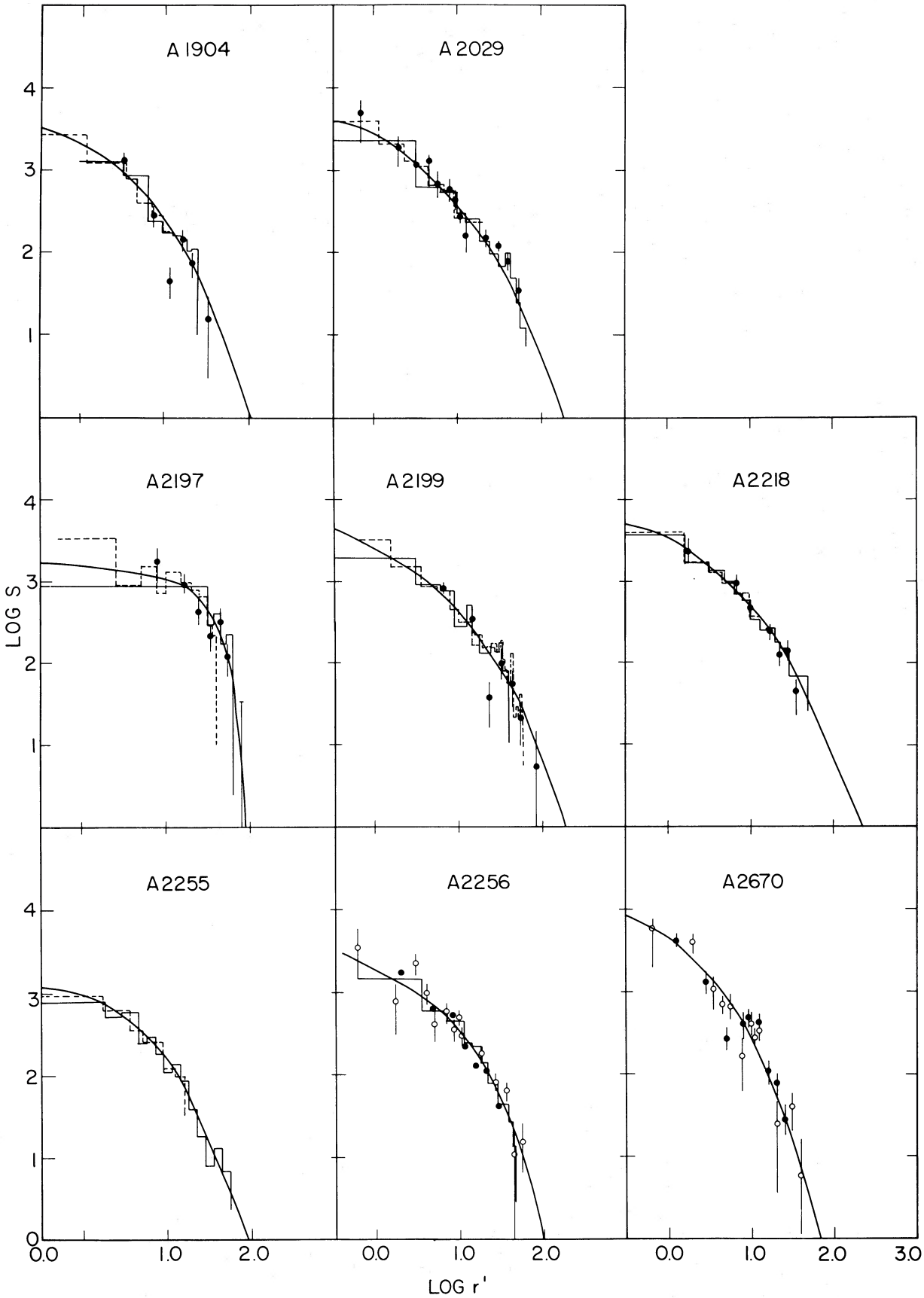

FIG. 12.—*Continued*

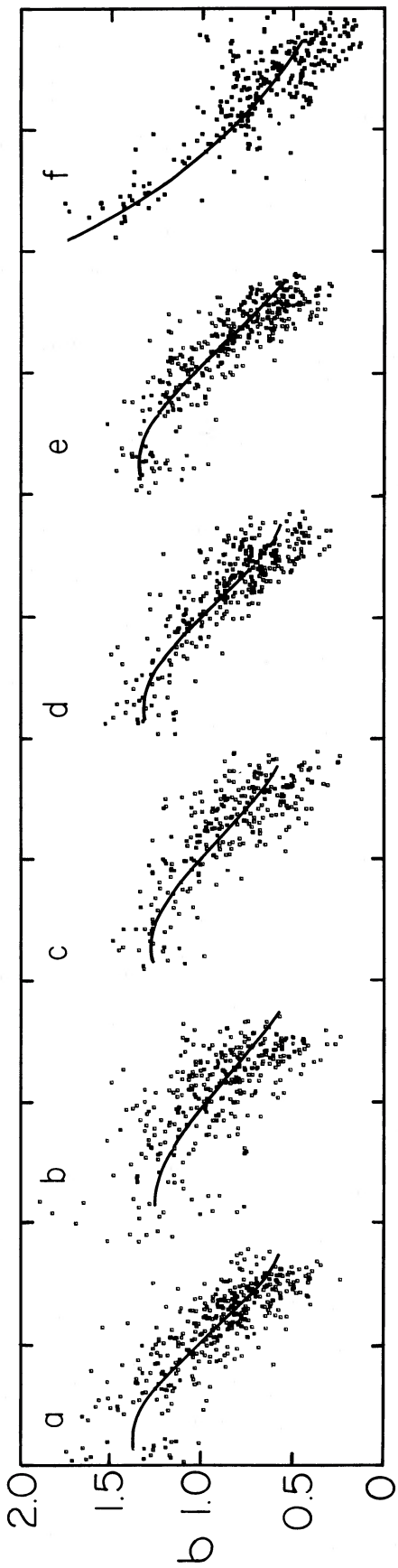

FIG. 13.—Line-of-sight velocity dispersion profiles of the simulated clusters. Velocity dispersions are in units of the global velocity dispersion. Curve labels are the same as in Fig. 3. Solid lines are best fits of a fourth-order power-series polynomial.

those of most clusters (Oemler 1974). Six clusters which have such profiles have not been used in any subsequent analysis: Abell 1228, 1367, 2197, and the Hercules and Virgo clusters. Such clusters are discussed in § IV.

IV. MASS PROFILES VERSUS LUMINOSITY PROFILES

As can be seen in Figures 3 and 4, the shapes of the projected mass density profiles of the simulated clusters with $\Omega = 1$ agree well with the observed galaxy count profiles of the sample of Abell clusters. This similarity of the profile shapes is confirmed in a more quantitative way by comparing the values of α_i in Table 1.

The simplest interpretation of this similarity between the theoretical profiles and the observed ones is that the radial mass distribution in clusters is similar to that of the light, thus showing no evidence for segregation between the dark and luminous matter in clusters. Any such segregation, if it existed at all, must have been smeared out by cluster evolution. Note, however, that the present simulations lack detailed physics in the cores, as discussed in § III. Such processes as dynamical friction, mergers, and mass segregation may tend to increase the concentration of luminous matter in the central regions.

It is worth mentioning here that none of our simulated clusters have profiles which are similar to those of the small subset of Abell clusters having very flat profiles. We have looked at a few clusters of lower densities in both the pancake and $n = 0$, $\Omega = 1$ hierarchical simulations, but found their profiles to be indistinguishable from those of the richer clusters. If this observed subset of clusters was simply the result of observing clusters at an early stage of evolution, we should have found such profiles when the model clusters were examined at earlier stages of the simulations (see Fig. 7). The significance of such clusters, and of their absence from our simulations, is not clear. It is possible that none of the cosmological models studied here can account for the whole variety of clusters in the real universe.

V. VELOCITY DISPERSION PROFILES

a) *Model Velocities*

Kent and Gunn (1982) and Kent and Sargent (1983) have studied the dynamics of the two rich clusters Coma and Perseus. They point out that systems with very different internal dynamics can yield almost indistinguishable density profiles, and for this reason it is important to examine the velocity dispersion profiles of clusters whenever possible. By comparing observational data of surface-brightness and line-of-sight velocity dispersion profiles with simple dynamical models, they concluded that in Coma, the assumption of constant mass-to-light ratio is consistent with an isotropic velocity distribution, while in Perseus, a constant mass-to-light ration can be obtained only if the velocity distribution is anisotropic, with galaxy orbits becoming increasingly radial with increasing distance beyond several core radii.

In Figure 13, we show line-of-sight velocity dispersion profiles of the simulated clusters, along with the best-fit curves to the data for each scenario. The particles have been binned in the identical manner as used to compute the mass density profiles, and the velocity dispersion of each bin normalized by the global cluster velocity dispersion. The simulated volume is small enough that contamination by foreground or background particles should be negligible. As can be seen, these profiles are quite similar for all of the models, with the exception of the open universe clusters, which tend to have steeper profiles in the innermost regions.

To address the question of isotropy of the velocity distribution, Figure 14 shows the ratio of the one-dimensional tangential to radial components of velocity, v_t/v_r, as a function of radius for clusters formed in two representative scenarios, the pancake and the $n = 0$, $\Omega = 1$ hierarchical clustering. For an isotropic distribution, this ratio should have a value of unity. It appears that all of the clusters have a fairly isotropic velocity distribution out to at least twice the half-mass radius. The clusters in the two scenarios show a certain degree of velocity anisotropy at larger radii, with $v_t/v_r \approx 0.6$ at 3 times the half-mass radius. The fact that the velocity distribution in the pancake clusters does not become very anisotropic at large radii may reflect the motion associated with pancake collapse, which should increase the tangential component of velocity for particles at large distances from the cluster center.

b) *Observed Profiles*

There are, unfortunately, many fewer data available on the internal kinematics of clusters than on their structure. We have found only five clusters for which there exists sufficient velocity dispersion profiles. These are the Coma Cluster (Kent and Gunn 1982), Perseus Cluster (Kent and Sargent 1983), Fornax Cluster (Mayall and de Vaucouleurs 1962; Welch, Chincarini, and Rood 1975; Jones and Jones 1980), Hydra Cluster (Richter, Materne, and Hutchmeier 1982), and Abell 194 (Chincarini and Rood 1971). We have subdivided the data for a cluster into between two and seven radial zones, and, in each zone, have calculated the velocity dispersion by a technique which is insensitive to contamination by foreground and background galaxies. We assume a Gaussian velocity distribution, discard all velocities which differ from the cluster mean by more than some value D, chosen to minimize background contamination, and calculate the velocity dispersion by a maximum likelihood method. Although statistically less efficient than the usual approach of discarding 3 σ points, it is less subject to systematic errors. This is especially important in the outer parts of a cluster, where contamination by noncluster members can be quite significant.

c) *Comparison of Theory and Observations*

In Figure 15, we have combined the five profiles, scaling them by R_{50}, and with the velocity dispersion scaled to achieve the best eye-fit. Within the errors, the shapes of the velocity profiles seem to be consistent with each other. This result is in contrast to that reached by Kent and Sargent (1983), who saw significant differences between the profiles of Coma and Perseus. The difference in our conclusions seem to be due mostly to the different methods of handling interlopers.

The theoretical velocity curves of the $\Omega = 1$ clusters are found to provide a reasonably good fit to the observational data, while the velocity profiles found for clusters formed in the open model are steeper in the inner regions than the observed profiles. This result provides an argument for $\Omega = 1$, and along with the similarity of the density profiles, it supports the contention that the overall mass distribution is the same in both the model and the Abell clusters, and that the isotropy profile of the velocity dispersion in the observed clusters can also be deduced from the models; it is quite isotropic inside twice the half-mass radius, and it becomes slightly radial outside.

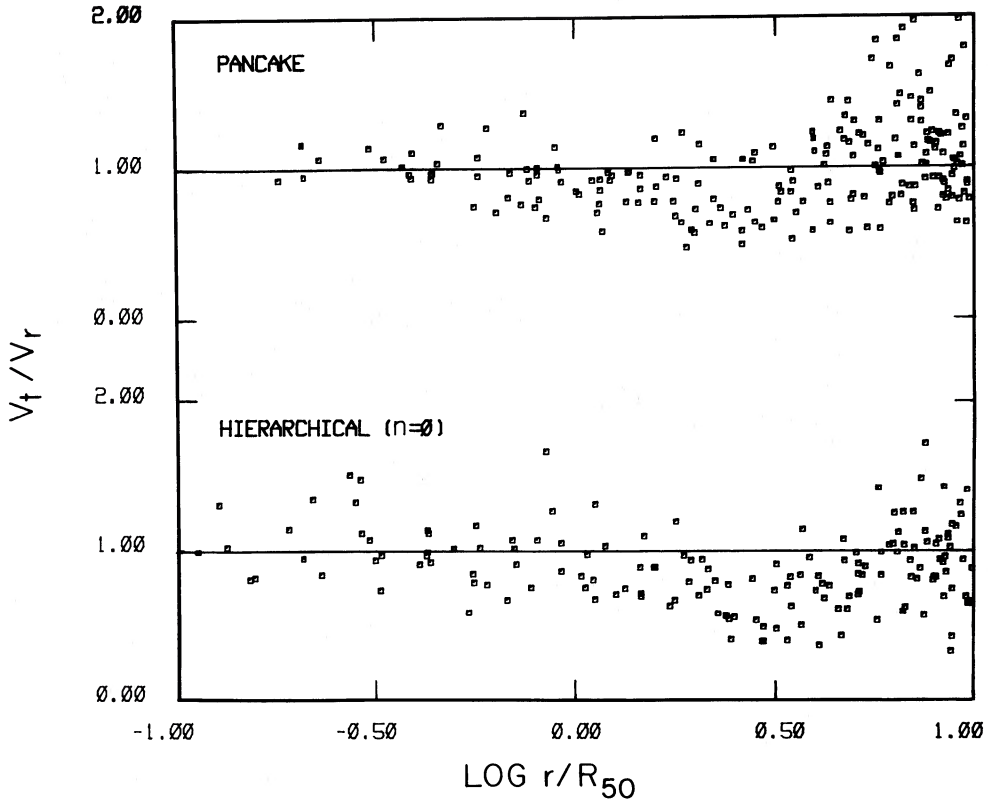

FIG. 14.—Ratio of one-dimensional tangential and radial components of velocity as a function of radius for clusters and surrounding regions in the pancake and $n = 0, \Omega = 1$ hierarchical clustering scenarios. No corrections have been made for contamination by neighboring clusters.

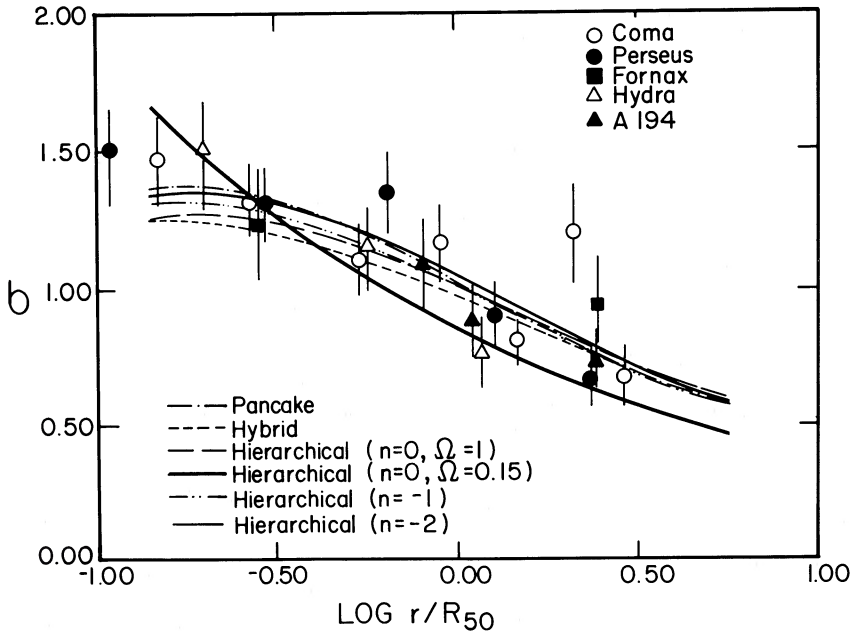

FIG. 15.—Line-of-sight velocity dispersion profiles of five Abell clusters. Observed velocity dispersions have been scaled to achieve a good eye-fit.

VI. CONCLUSIONS

We have studied the profiles of rich clusters of galaxies formed in various cosmological scenarios by comparing the results of high-resolution N-body simulations with observations of a sample of 27 Abell clusters.

The cluster mass density profiles obtained from a wide range of initial conditions are found to be quite similar in shape and scaling. This suggests that dynamical effects such as violent relaxation are efficient at erasing traces of the initial conditions from the final radial mass distribution in clusters. The fact that we find a universal theoretical mass density profile indicates that such profiles do not provide a useful test for distinguishing between the competing scenarios for the formation of the large-scale structure in the universe. However, we do find a slight tendency for somewhat steeper profiles in the inner regions of clusters formed in an open universe, although determining whether or not this is a significant difference requires more detailed simulations.

The theoretical mass density profiles and the observed surface brightness profiles are found to be quite similar. The simplest interpretation of this result is that the ratio of luminous to nonluminous matter does not vary with radius in rich clusters of galaxies, on scales of 1–2 h^{-1} Mpc.

Similarly, we have examined the velocity dispersion profiles of the simulated clusters, and compared these to the observed profiles of a small sample of Abell clusters. The theoretical velocity dispersion profiles are found to be quite similar in all the different scenarios with $\Omega = 1$, and these agree with the limited observations available at present. The clusters formed in an open universe show velocity profiles which are too steep. More detailed and systematic studies of rich clusters are needed in order to confirm these results. We find that the velocity distribution of the simulated clusters is quite isotropic out to fairly large radii.

Other clusters properties are presently being examined, and preliminary results indicate that several of them may provide a more sensitive test of the cosmological secenario in which the clusters formed. We discuss these in Papers II and III, in which we study such measures as cluster ellipticities, subclustering, binding energies, and others.

We thank Sverre Aarseth for allowing the use of his N-body codes, Julio Ortiz for his help with the observational data, and Erez Braun for his help in testing the initial conditions.

APPENDIX A

GAUSSIAN REALIZATION OF THE INITIAL SPECTRUM

The goal is to represent a random-phase realization of a given initial power spectrum of small density fluctuations,

$$P(k) = \langle |\tilde{\delta}(\boldsymbol{k})|^2 \rangle , \tag{A1}$$

in a range $k_{\min} < k < k_{\max}$, by appropriately distributing N particles in the volume V to be simulated (e.g., a unit sphere), without necessarily requiring periodic boundary conditions. Using the Zel'dovich (1970) approximation at the starting time t, the particles are first distributed uniformly inside the volume, at the points of a cubic grid. The comoving position of each particle, $\boldsymbol{q}$, is then slightly displaced by

$$-b(t)\psi(\boldsymbol{q}) , \tag{A2}$$

where $b(t)$ is constant in space which grows in time as $b(t) \propto t^{2/3}$, as long as $\Omega = 1$. In the case of "adiabatic" fluctuations, each particle is given a corresponding peculiar velocity relative to the Hubble flow (in comoving units) of

$$-\dot{b}(t)\psi(\boldsymbol{q}) , \tag{A3}$$

representing only the growing modes.

The spatial perturbation $\psi(\boldsymbol{q})$ is taken to be the superposition of N_k small-amplitude plane waves,

$$\psi(\boldsymbol{q}) = \sum_{i=1}^{N_k} \sin(\boldsymbol{k}_i \cdot \boldsymbol{q} + \phi_i) \frac{\boldsymbol{k}_i}{k_i^2} \left[\frac{P(k_i)}{w(k_i)}\right]^{1/2} . \tag{A4}$$

The corresponding density fluctuation is

$$\delta(\boldsymbol{q}) = 1 \Big/ \det\left[\delta_{jk} - b(t)\frac{\partial \psi_j}{\partial q_k}\right] - 1 , \tag{A5}$$

which, in the linear approximation ($b\psi \ll q$), is simply

$$\delta(\boldsymbol{q}) = b(t) \sum_{j=1}^{3} \frac{\partial \psi_j}{\partial q_j} = b(t) \sum_{i=1}^{N_k} \cos(\boldsymbol{k}_i \cdot \boldsymbol{q} + \phi_i) \left[\frac{P(k_i)}{w(k_i)}\right]^{1/2} . \tag{A6}$$

The phases ϕ_i are chosen uniformly at random in the interval $(0, 2\pi)$. The directions of the wave vectors, $\boldsymbol{k}_i$, are chosen uniformly at random. Their amplitudes, k_i, are chosen at random within $(k_{\min}, k_{\max})$ such that the number density of waves is $w(k)$. In practice, we select the k values via function $u(k)$ which satisfies

$$w(k)d^3k = \frac{N_k}{u(k_{\max}) - u(k_{\min})} du(k) . \tag{A7}$$

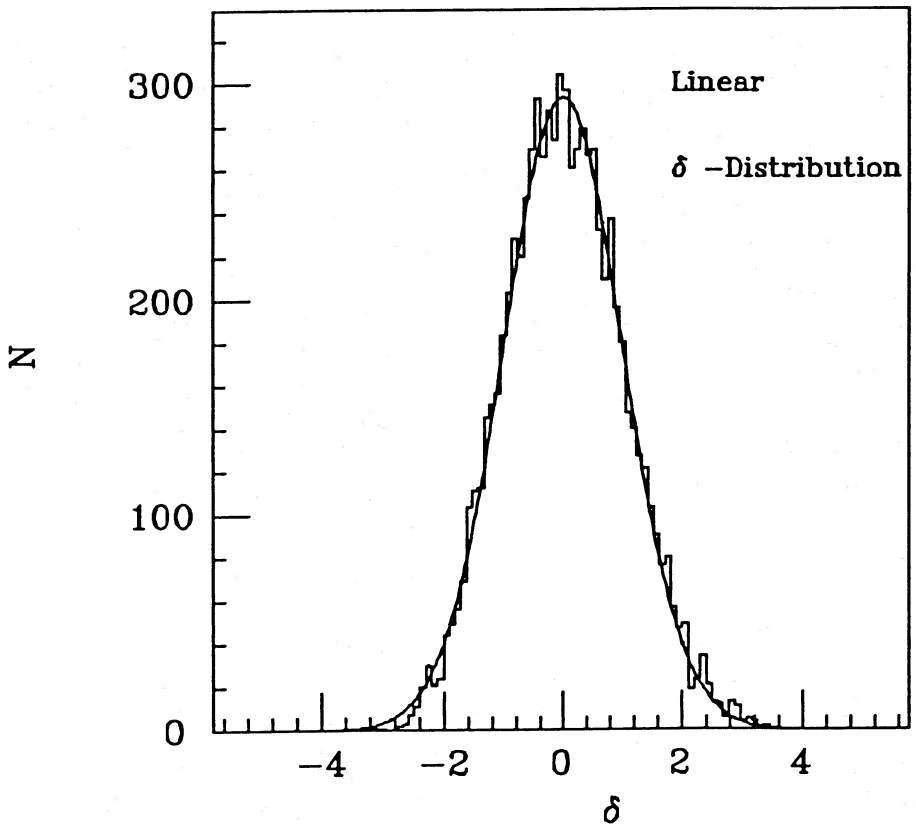

FIG. 16.—Histogram distribution of $\delta(q)/\langle\delta^2\rangle^{1/2}$ over 8000 grid points in the initial conditions ($\varepsilon \ll 1$), compared with a Gaussian distribution over 8000 points

The values of $u(k)$ are chosen uniformly at random in the interval $u(k_{\min}) \leq u(k) \leq u(k_{\max})$, and the corresponding wavenumbers k are used in the superposition.

The weight function $w(k)$ could, in principle, be arbitrary. For example, the choice $w(k)$ = constant, corresponding to $u(k) = k^3$, would give a uniform coverage of the three-dimensional k-space. This choice is equivalent to the use of a cubic grid in k-space, which is forced when periodic boundary conditions are imposed and Fourier transforms are calculated (Efstathiou *et al.* 1985). But the representation of the spectrum for small k's (large scales) is very poor in such a case. A much more "uniform" representation of the spectrum over the whole range ($k_{\min}$, $k_{\max}$) is achieved with an equal number of waves per logarithmic interval in k, i.e.

$$u(k) = \ln k \,, \tag{A8}$$

which corresponds to

$$w(k) = \frac{N_k}{4\pi(\ln k_{\max} - \ln k_{\min})} k^{-3} \,. \tag{A9}$$

By increasing N_k, the number of waves increases in the same way in every ln k interval, so the discrete spectrum approaches a continues one in k; there is no need in this case to distribute the amplitudes of $\tilde{\delta}(\boldsymbol{k})$ normally about their mean. The randomly chosen phases guarantee that the contribution to δ from every small ln k interval is normal, such that δ approximates a Gaussian process. Figure 16 shows a histogram of the distribution of δ (normalized to $\langle\delta^2\rangle = 1$), as calculated by equation (A-6) over 8000 grid points inside a unit sphere. With $N_k = 1000$ and $k_{\max}/k_{\min} = 10$ we have 30 waves per each 7% k interval. The figure shows how well the initial conditions indeed approximate a Gaussian distribution.

The desired fluctuations are represented well down to a comoving wavelength corresponding to twice the initial grid points separation,

$$\lambda_{\min} = 2\pi/k_{\max} = 2(V/N)^{1/3} \,. \tag{A10}$$

In our cluster simulations $\lambda_{\min} \approx 0.1$, corresponding to $\sim 5\, h^{-1}$ Mpc in comoving units. In the collapsed clusters of the hierarchical clustering scenarios, the material in the relevant range of radii, 0.5–5 h^{-1} Mpc, have collapsed from comoving radii in the range 8–14 h^{-1} Mpc, scale on which the initial spectrum of fluctuations is represented well.

Finally, the mean square fluctuation averaged over spheres of diameter λ is

$$\langle\delta^2\rangle_\lambda \approx (\tfrac{1}{2})b^2(t) \int_{k_{\min}}^{1/\lambda} P(k) d^3k \,. \tag{A11}$$

The quantities $P(k)$ and $b(t)$ are normalized such that on a certain scale, λ_u (e.g. the coherence length in the neutrino scenario),

$$\langle \delta^2 \rangle_{\lambda_u} = b^2(t) \, . \tag{A12}$$

This procedure of generating the initial conditions is to be discussed in more detail elsewhere (Dekel 1986*b*, in preparation). Various tests were performed to estimate how well it reproduces the desired initial spectrum of fluctuations and the random phases within the desired range of scales. In one test, for example, the local linear density contrast (eq. [A6]), is fast-Fourier transformed back to k-space and compared to the original spectrum. In another test the two-point correlation function in the linear regime, as obtained from pair counts, is compared with that calculated by Fourier transforming the power spectrum. These tests and others show that the procedure used here does reproduce the desired initial fluctuations to a good accuracy.

REFERENCES

Aarseth, S. J. 1984, in *Method of Computational Physics*, ed. J. U. Brackbill and B. I. Cohen (New York: Academic), p. 1.
Bahcall, N. A. 1973, *Ap. J.*, **186**, 1179.
———. 1974, *Ap. J.*, **187**, 439.
———. 1975, *Ap. J.*, **198**, 249.
Bahcall, N., and Soneira, R. M. 1983, *Ap. J.*, **270**, 20.
Baier, F. N. 1978, *Astr. Nach.*, **299**, 311.
Bardeen, J. M., Bond, J. R., Kaiser, N., and Szalay, A. S. 1986, *Ap. J.*, **304**, 15.
Beers, T. C., and Tonry, J. L. 1986, preprint.
Binggeli, B. 1982, *Astr. Ap.* **107**, 338.
Butcher, H., and Oemler, A., Jr. 1978, *Ap. J.*, **226**, 559.
———. 1984, *Ap. J.*, **285**, 426.
Chincarini, G., and Rood, H. J. 1971, *A.J.*, **77**, 4.
Davis, M., Efstathiou, G., Frenk, C. S., and White, S. D. M. 1985, *Ap. J.*, **292**, 371.
Davis, M., and Peebles, P. J. E. 1983, *Ap. J.*, **267**, 465.
Dekel, A. 1981, *Astr. Ap.*, **101**, 29.
———. 1983, *Ap. J.*, **264**, 373.
———. 1984, in *Proc. 8th Johns Hopkins Workshop on Current Problems in Particle Theory, Particles, and Gravity*, ed. G. Domokos and S. Kovesi-Domokos (Singapore: World Scientific), p. 191.
———. 1986*a*, *Comments Ap.*, **11**, 235.
———. 1986*b*, in preparation.
Dekel, A., and Aarseth, S. J. 1984, *Ap. J.*, **283**, 1.
Dekel, A., Kowitt, J., and Shaham, J. 1981, *Ap. J.*, **250**, 561.
Dekel, A., and Shaham, J. 1980, *Astr. Ap.*, **85**, 154.
Dekel, A., and Silk, J. 1986, *Ap. J.*, April 15, in press.
Dekel, A., West, M. J., and Aarseth, S. J. 1984, *Ap. J.*, **279**, 1.
de Vaucouleurs, G., de Vaucoulers, A., and Corwin, H. G. 1976, *Second Reference Catalogue of Bright Galaxies* (Austin: University of Texas Press).
Doroshkevich, A. G. 1970, *Astrophysics*, **6**, 320.
Dressler, A. 1978, *Ap. J.*, **226**, 55.
———. 1980, *Ap. J.*, **236**, 351.
Duus, A. 1977, Ph.D. thesis, Australian National University.
Efstathiou, G., Davis, M., Frenk, C. S., and White, S. D. H. 1985, *Ap. J. Suppl.*, **57**, 241.
Einasto, J., Klypin, A. A., Saar, E., and Shandarin, S. F. 1984, *M.N.R.A.S.*, **206**, 529.
Farouki, R. T., Hoffman, G. L., and Salpeter, E. E. 1984, *Ap. J.*, **271**, 11.
Fillmore, J. A., and Goldreich, P. 1984, *Ap. J.*, **281**, 1.
Frenk, C. S., White, S. D. M., Efstathiou, G., and Davis, M. 1986, preprint.
Gott, J. R. 1975, *Ap. J.*, **201**, 296.
Gunn, J. E. 1977, *Ap. J.*, **218**, 592.
Gunn, J. E., and Gott, J. R. 1972, *Ap. J.*, **176**, 1.
Hoffman, Y., and Shaham, J. 1985, *Ap. J.*, **297**, 16.
Jones, J. E., and Jones, B. J. T. 1980, *M.N.R.A.S.*, **191**, 685.
Kaiser, N. 1984, *Ap. J. (Letters)*, **284**, L9.
Kent, S. M., and Gunn, J. E. 1982, *A.J.*, **87**, 945.
Kent, S. M., and Sargent, N. L. N. 1983, *A.J.*, **88**, 697.
Kirshner, R. P., Oemler, A., Schechter, P. L., and Shectman, S. A. 1984, *A.J.*, **88**, 1285.
Kwast, T. 1966, *Acta Astr.*, **16**, 45.
Lynden-Bell, D. 1967, *M.N.R.A.S.*, **136**, 101.
Malumuth, E. M., and Richstone, D. O. 1984, *Ap. J.*, **276**, 413.
May, A., and van Albada, T. S. 1984, *M.N.R.A.S.*, **209**, 15.
Mayall, N. U., and de Vaucouleurs, A. 1962, *A.J.*, **67**, 363.
Merritt, D. 1984, *Ap. J.*, **276**, 26.
Noonan, T. 1973, *A.J.*, **78**, 26.
Oemler, A. 1974, *Ap. J.*, **194**, 1.
Omer, G. C., Page, T. L., and Wilson, A. G. 1965, *A.J.*, **70**, 6.
Ostriker, J. 1977, *Ap. J. (Letters)*, **217**, L15.
Peebles, P. J. E. 1970, *A.J.*, **75**, 13.
———. 1982, *Ap. J. (Letters)*, **263**, L1.
———. 1986, *Nature*, in press.
Peebles, P. J. E., and Dicke, R. 1968, *Ap. J.*, **154**, 891.
Pryor, C., and Lecar, M. 1983, *Ap. J.*, **269**, 513.
Quinn, P. J., Salmon, J. K., and Zurek, W. H. 1986, preprint.
Quintana, H. 1979, *A.J.*, **84**, 15.
Rees, M. J. 1985, *M.N.R.A.S.*, **213**, 75p.
Rees, M. J., and Dekel, A. 1986, *Nature*, submitted.
Richstone, D. O., and Malumuth, E. M. 1983, *Ap. J.*, **268**, 30.
Richter, O. G., Materne, J., and Hutchmeier, N. K. 1982, *Astr. Ap.*, **111**, 193.
Silk, J. 1985, *Ap. J.*, **297**, 1.
Strubles, M. F., and Peebles, P. J. E. 1985, *A.J.*, **90**, 582.
van Albada, T. S. 1982, *M.N.R.A.S.*, **201**, 939.
Villumsen, J. V. 1984, *Ap. J.*, **284**, 75.
Welch, Chincarini, and Rood, H. J. 1975, *A.J.*, **80**, 77.
West, M. J., Dekel, A., and Oemler, A. 1986*a*, in preparation (Paper II).
———. 1986*c*, in preparation (Paper III).
White, S. D. M. 1976, *M.N.R.A.S.*, **177**, 717.
Yahil, A. 1974, *Ap. J.*, **191**, 623.
Zel'dovich, Ya. B. 1970, *Astr. Ap.*, **5**, 84.
Zwicky, F. 1937, *Ap. J.*, **86**, 217.
———. 1956, in *Proc. 3d Berkeley Symposium on Mathematical Statistics*, ed. J. Neyman (Berkeley: University of California), p. 113.
———. 1957, *Morphological Astronomy* (Berlin: Springer-Verlag).

AVISHAI DEKEL: Racah Institute of Physics, Hebrew University, Jerusalem 91904, Israel

AUGUSTUS OEMLER, JR: Department of Astronomy, Yale University, P.O. Box 6666, New Haven, CT 06511

MICHAEL J. WEST: Department of Astronomy, University of Michigan, Dennison Building, Ann Arbor, MI 48109